Chapter 41
Methanol and CO electrooxidation

T. Iwasita
Instituto de Quimica de São Carlos, USP, São Carlos-SP, Brazil

1 INTRODUCTION

The methanol oxidation reaction has been the subject of a large number of studies in the past.[1, 2] Early work revealed a complex reaction mechanism,[3–6] indicating the electrocatalysis of methanol oxidation as the most difficult task in the realization of a direct methanol fuel cell (DMFC). Several metal catalysts were proposed for the reaction, most of them based on modifications of Pt with some other metal.[7–10]

For about 15 years, research on the DMFC has been receiving great attention (see **Direct methanol fuel cells (DMFC)**, Volume 1). Considerable effort has been devoted to the technical realization of the methanol fuel cell and a wealth of basic research has been directed to elucidate the mechanistic aspects of methanol oxidation. In fact, methanol and other small organic molecules have been studied for more than 70 years, but a greater understanding was achieved by the development of ex situ and in situ spectroscopic and microscopic methods for application in electrochemistry,[11–14] together with the use of well-defined monocrystalline electrode surfaces.[15]

This chapter presents a state-of-the-art review on the electrocatalysis of methanol oxidation. Research on methanol, as well as on the parent compounds formaldehyde and formic acid, has been reviewed several times (see for example, Refs. [16–18]). Therefore, this discussion is centered on those aspects of the electrocatalysis of methanol oxidation which are at present well established or which may need further investigation. The purpose of this contribution is to present our current understanding of the methanol system and provide a basis for future investigations. It is with this objective in mind, that the references in this chapter were selected. Nevertheless, as in any paper of this kind, it is unavoidable that the criteria of the author prevail and therefore, for thorough literature research, the reader is directed to the excellent reviews in Refs. [16–18].

Thermodynamic data for methanol, carbon monoxide and other small organic molecules are given in Table 1.[1] Accordingly, their thermodynamic open circuit potentials are of the same order as that of hydrogen and these substances can be considered good candidates to operate as anode material in a fuel cell. However, while hydrogen oxidation occurs at relatively high rates near its reversible potential, the oxidation of small organic molecules presents serious kinetic limitations. As an example, in Figure 1, the response of a Pt electrode to a constant current step of 5 mA in a methanol-containing solution is compared with that of hydrogen (1 bar) in the same base electrolyte (0.5 M H_2SO_4). Whilst at such high rates hydrogen oxidation exhibits a small overpotential, for methanol oxidation the potential is shifted to very high values (0.55 V) only a few seconds after applying the potential step.

The results shown in Figure 1, illustrating the behavior of pure Pt towards methanol oxidation, indicate that this pure metal could never be a good catalyst for continuous fuel cell (FC) operation at room temperature or even higher (e.g., 60 °C). However, in spite of the problem of being strongly poisoned by adsorption products, no better catalyst than Pt for breaking C–H and O–H bonds in alcohol molecules is known at present. Therefore, methanol electrooxidation at reasonable rates in acid media is only conceivable on Pt-based catalysts. Research in electrocatalysis using modified Pt electrodes has devoted considerable

Handbook of Fuel Cells – Fundamentals, Technology and Applications, Edited by Wolf Vielstich, Hubert A. Gasteiger, Arnold Lamm. Volume 2: *Electrocatalysis*. ISBN: 0-471-49926-9.

Table 1. Thermodynamic data on the oxidation of CO, methanol and related substances at 25 °C and 1 atm.[1]

Theoretical cell reaction	ΔH° (kcal mol^{-1})	ΔS° (cal mol^{-1})	ΔG° (kcal mol^{-1})	n	E° (V)
$H_2 + O_2 \rightarrow H_2O$ (liq)	−68.14	−39.0	−56.69	2	1.23
$C + \frac{1}{2}O_2 \rightarrow CO$	−26.4	+21.4	−32.81	2	0.71
$CO + \frac{1}{2}O_2 \rightarrow CO_2$	−67.62	−20.7	−61.45	2	1.33
$CH_3OH + \frac{3}{2}O_2 \rightarrow CO_2 + 2H_2O$	−173.8	−23.5	−166.8	6	1.21
$CH_2O + O_2 \rightarrow CO_2 + H_2O$	−134,28	−32.1	−124.7	4	1.35
$HCOOH + \frac{1}{2}O_2 \rightarrow CO_2 + H_2O$	−64,66	+11.8	−68.2	2	1.48

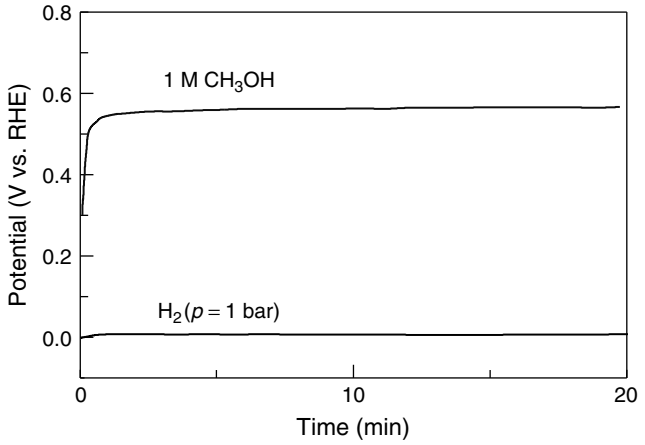

Figure 1. Potential as a function of time for a platinized Pt electrode, at a constant current of 5 mA in solutions of 1.0 M $CH_3OH + 0.5$ M H_2SO_4 and 0.5 M H_2SO_4 saturated with H_2 (1 bar). Room temperature. (Reproduced from Iwasita (1990)[11] with permission from VCH.)

effort to the study of oxidation of the (main) adsorbed residue of methanol, carbon monoxide. Summarizing, an important, although not unique aspect of the catalysis of methanol oxidation is related to the catalysis of CO oxidation. Therefore, methanol and CO oxidation reactions are both discussed in this chapter. For practical reasons, the chapter is divided into two sections, devoted to carbon monoxide and methanol, respectively.

2 OXIDATION OF CARBON MONOXIDE

Carbon monoxide is one of the most studied species in surface science. In electrochemical environments carbon monoxide is often used as a probe molecule for vibrational spectroscopy and scanning tunneling microscopy (STM).[19, 20] Such studies permitted a link to be established between the behavior of the metal in the gas phase and in the electrochemical environment, thus aiding the understanding of the physicochemical properties of electrode surfaces and adsorbed species in the double layer. The reader may find interesting contributions on this issue in Refs. [21–23].

Although, as explained before, CO was found to be a poisoning adsorbate during the oxidation of small organic molecules,[12] in early studies CO itself was studied as a candidate for driving an alkaline fuel cell.[1]

In this section, we describe some aspects of carbon monoxide oxidation which are relevant for the electrocatalysis of fuel cell reactions. At present, the main interest of CO oxidation is centered on two practical problems involving the use of Pt-based catalysts: (i) the development of CO-tolerant H_2 anodes for the H_2/O_2 acid fuel cell (see for example Ref. [24]) and (ii) the search for a catalyst for methanol oxidation in acid media. In the first case, CO can be present as a by-product in the gaseous H_2 produced by reformation of hydrocarbons or alcohols. This problem is thoroughly discussed in **New CO-tolerant catalyst concepts**, Volume 2. In the case of methanol, CO formed during dissociative adsorption on pure Pt covers a considerable fraction of the electrode surface in a matter of seconds. At potentials below 0.4 V, the reaction cannot progress due to the inability of platinum to form OH for further oxidation and the current falls to negligible values. For this reason CO_{ad} was considered to be a catalyst "poison", a term that may have to be revised as discussed later in this chapter.

An interesting feature concerning CO electrooxidation on Pt electrodes is that much higher overpotentials are required for stripping a CO adlayer in pure supporting electrolyte than for oxidizing CO molecules present in the bulk of the solution. This result can be paralleled with the results of gas phase experiments at Pt(100) showing that oxidation of gaseous CO with adsorbed oxygen occurs with a probability of one, while chemisorbed CO is virtually unreactive.[25] (At first, it was proposed that the reaction follows a Rideal–Eley mechanism, but since the reaction continues to occur with probability one at very low CO

pressure, when the collision probability between CO and oxygen is much smaller, it was concluded that the reaction occurs via a Langmuir–Hinshelwood mechanism, by forming a (reactive) *precursor* state.[26])

The remainder of Section 2 is divided into three subsections: (1) oxidation of adsorbed CO at Pt electrodes; (2) CO oxidation in the presence of dissolved CO; and (3) effect of electronegative adatoms on CO oxidation.

2.1 Oxidation of CO adlayers on pure platinum

The oxidative behavior of carbon monoxide at Pt is dependent on several experimental parameters. Among others, the adsorption potential, the degree of coverage and the presence of CO in the bulk of the electrolyte strongly affect the rate of reaction.[27–31]

In Figure 2 we show stripping voltammetry of saturated CO adlayers formed on a Pt(111) electrode at (a) 0.37 V and (b) 0.05 V.[31] Experiments were performed in 0.1 M $HClO_4$. After adsorption, CO was eliminated from the solution by bubbling argon. There is a clear difference in the onset potential of CO oxidation. Thus, for adsorption at 0.37 V only one peak, at 0.74 V, is observed. On the other hand, for CO adsorption at 0.05 V, in addition to the sharp peak by ca. 0.74 V, a small *pre-peak*, at around 0.5 V is present. The presence of this feature, which is only observed when the Pt surface becomes saturated with CO at low adsorption potentials (below 0.3 V), is well documented in the literature. The pre-peak was also observed for saturated adlayers at low adsorption potentials on polycrystalline Pt[27, 32, 33] and on monocrystalline Pt(hkl) electrodes.[31, 34, 35] The existence of a pre-peak, with an onset potential of ca. 0.3 V, suggests that some CO molecules at the adlayer are, probably, weakly bonded to the surface.[11] Whether this state depends on the particular adsorption site (e.g., CO adsorbed on edges or on defect sites) cannot be documented at present. It should be recalled that, according to UHV data, the energy of adsorption of CO at Pt(hkl) is a function of the degree of coverage θ_{CO} and decreases very markedly as θ_{CO} reaches the saturation value for the respective surface.[36] If this result is extended to the electrochemical environment, the low potential for CO oxidation at the pre-peak can be due to oxidation of CO molecules having a low value of adsorption energy in the saturated adlayer. However, although the pre-peak represents a very low fraction of the total charge of the CO adlayer, it indicates the existence of a pathway for CO oxidation occurring at low potentials and this is important in terms of the catalysis of the reaction. As we discuss in the next section, experiments performed in the presence of bulk CO, after an admission potential of 0.05 V show an overlap of the peak for bulk oxidation with the pre-peak. This fact suggests that the sites involved in the process at the pre-peak could be the open door for bulk oxidation at low potentials.

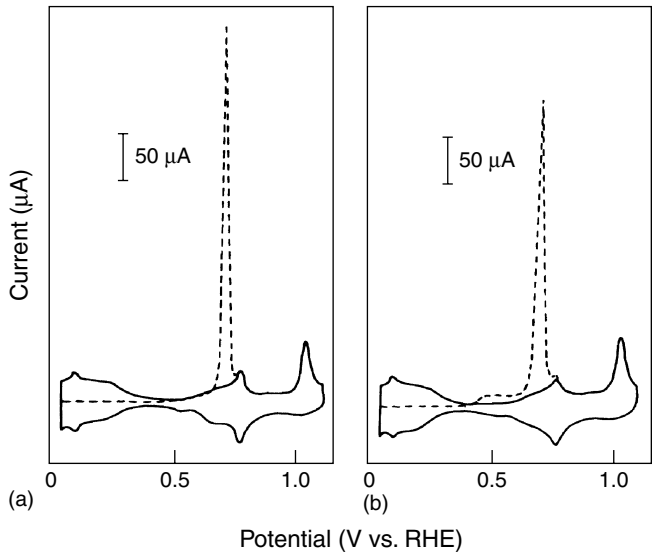

Figure 2. Stripping voltammetry of saturated CO adlayers in 0.1 M $HClO_4$ solution. Adlayers formed on a Pt(111) electrode at (a) 0.37 V and (b) 0.05 V. (Reproduced from Wieckowski *et al.* (1985)[31] with permission from Elsevier Science.)

Without consideration of the pre-peak, kinetic studies on CO oxidation at Pt refer mainly to the process occurring at high potentials. Gilman[37] was the first to propose that oxidation of CO involves the reaction between adsorbed CO molecules and an adsorbed O-containing species. The exact nature of this species is not yet sufficiently documented, although it is believed to be adsorbed OH coming from the dissociation of water.

Oxidation of CO in the gas phase, follows a Langmuir–Hinshelwood mechanism[25] involving adsorbed CO and co-adsorbed oxygen. The high mobility of adsorbed CO in the metal gas interface[38] is good support for this mechanism. At present, however, no experimental data on the surface diffusion of CO at electrodes are available and it is difficult to make estimates since the situation in the electrochemical cell could be different to that in UHV.

At electrochemical interfaces carbon monoxide is adsorbed forming islands and it was suggested that for the occurrence of a Langmuir–Hinshelwood mechanism the adsorbate must move to the places where OH is formed, namely to the Pt sites free of CO. According to a recent Monte Carlo study of the kinetics of CO_{ad} oxidation,[39] the adsorbate mobility is a necessary condition for a bimolecular surface reaction. Cyclic voltammetry (CV) and chronoamperometry have been used to study the mechanism of CO stripping.[40–43] It was suggested that the

reaction between CO_{ad} and OH_{ad} proceeds through a nucleation mechanism as a front at the edges of separate regions populated by the reactants.[40] The model responds to experimental current–time transients of McCallum and Pletcher,[41] for polycrystalline Pt, and Love and Lipkowski for Pt(111).[40] These authors observed a change in the form of the transient at high potentials together with a change in the Tafel slope. They explained this effect in terms of a transition from progressive to instantaneous nucleation.[40]

Petukhov *et al.*[43] also measured current transients for CO oxidation at Pt(111) and compared the results with data from the Monte Carlo simulation. These authors estimated a value of $5 \times 10^{-13}\,cm^2\,s^{-1}$ for the CO diffusion coefficient and concluded that, due to this low value, a simple Langmuir–Hinschelwood mechanism cannot occur at the electrochemical interface.[43]

According to Koper *et al.*[39] a reaction mechanism for CO oxidation can be written as follows:

$$H_2O + {}^* \longleftrightarrow OH_{ads} + H^+ + e^- \qquad (1)$$

$$CO_{ads} + OH_{ads} \longrightarrow CO_2 + H^+ + e^- + 2^* \qquad (2)$$

where * stands for a free site on the surface. Thus, the importance of the rate of OH adsorption-desorption (1) is enhanced. The change in Tafel slope mentioned above can be explained by considering the effect of the potential on this reaction. In addition, Koper *et al.*[39] show that experimental and simulated CV data only coincide if a high surface mobility is assumed for CO_{ad}.

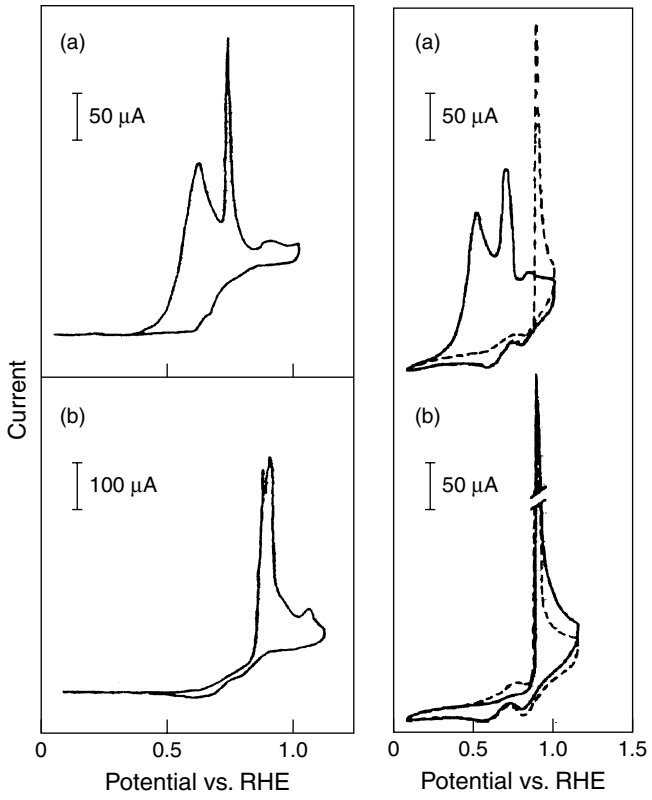

Figure 3. Cyclic voltammograms for Pt(111) (left) and polycrystalline Pt (right) in CO-saturated 0.1 M $HClO_4$ solutions. Left: scan rate, $20\,mV\,s^{-1}$; CO admission at +0.130 V vs. RHE; (a) first scan, (b) third scan. Right: scan rate, $50\,mV\,s^{-1}$; (a) admission potential 0.05 V vs. RHE, (b) admission potential 0.37 V vs. RHE. Solid line: first scan, dashed line tenth scan. (Reproduced from Wieckowski *et al.* (1985)[31] with permission from Elsevier Science.)

2.2 Oxidation of CO in the presence of dissolved CO

In the presence of dissolved CO in the bulk of the solution, a cyclic voltammogram exhibits higher oxidation currents during the first potential scan, if the admission potential is low (below 0.2 V). This behavior was reported for polycrystalline Pt and for single crystal Pt as well, and can be seen in Figure 3.[31] The onset potential of the oxidation current is comparable to that of the pre-peak and first oxidation peaks are observed at 0.63 V and 0.52 V for Pt(111) and polycrystalline Pt, respectively. This high electrode activity drastically falls when the admission potential is in the double layer region, e.g., at 0.37 V as in Figure 3 (right, b). It also falls during the second and subsequent scans as shown in Figure 3 (left, b). Evidently, some irreversible change occurs in the system at potentials above ca. 0.3 V, with negative consequences for the catalysis of CO oxidation.

Data from scanning tunneling microscopy (STM) and infrared spectroscopy,[19, 20, 44] indicate that on Pt(111) the onset of CO oxidation occurs simultaneously with a transition of the CO adlayer structure. Villegas and Weaver[19] discussed data from STM experiments (Figure 4) and in situ FTIR (Figure 5) for CO adsorbed on Pt(111) in the presence of dissolved CO. A change of potential from −0.05 V and +0.4 V vs. RHE (in the original paper,[19] these potentials are given as −0.25 and +0.1 V vs. SCE) induces a transition in the adlayer structure, as shown in Figure 4. The unit cells at 0.05 V and 0.4 V vs. RHE are respectively (2×2)−3CO and $(\sqrt{19} \times \sqrt{19})23.4^\circ$−13CO. The transition is accompanied by a change in the spectra as shown in Figure 5. IR bands correspond to terminal ($2073\,cm^{-1}$), bridge ($1850\,cm^{-1}$) and three-fold ($1773\,cm^{-1}$) bonded CO.[19] Summarizing, at −0.05 V vs. RHE CO presents a (2×2)−3CO structure occupying on top and threefold hollow sites, while at 0.4 V vs. RHE the adlayer consists of a $(\sqrt{19} \times \sqrt{19})R23.4^\circ$−13CO structure with CO molecules occupying on top and two fold bridge positions.

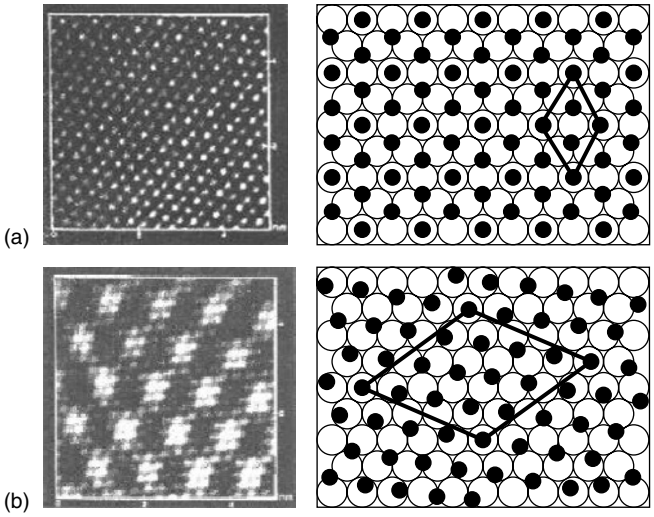

Figure 4. STM images and ball models of adsorbed CO at Pt(111), taken in the presence of dissolved CO. (a) $(2 \times 2)-3CO$ and (b) $(\sqrt{19} \times \sqrt{19})23.4^{\circ}-13CO$. Scales: 5×5 nm. (Reproduced from Villegas and Weaver (1994)[19] with permission from the American Institute of Physics.)

Two important points concerning the results of Figures 4 and 5 are noteworthy:

- Strong dipole-dipole coupling in the highly compressed (2×2) layer gives rise to a considerable intensity transfer from the multifold CO molecules to terminal CO.[19] As a consequence the 2 : 1 site occupancy in favor of multifold CO geometry shown by the STM picture is not reflected in the band intensities of the IR spectra, which favors the minority atop molecules.[19] In other words, these results prevent us from establishing the relative degree of coverage by comparing the respective band intensities.
- The change from the (2×2) to the $(\sqrt{19} \times \sqrt{19})$ structure was reported in different other works at different potentials between 0.4 V and 0.65 V vs. RHE.[20, 44, 45] It was shown that these differences lie in the degree of order of the Pt(111) surface.[44] Thus, on ordered surfaces, presenting wide terraces and few steps, the transition occurs at ca. 0.6 V, while stepped or disordered surfaces cause a shift of the transition to lower potentials. Regarding the catalysis of CO oxidation, it is important to note that the adlayer transition is accompanied by CO_2 formation,[20, 44] and this fact highlights the role of steps in the catalysis of the reaction.

Yoshimi *et al.* reported a differential behavior of the CO adlayer for CO adsorbed at 0.4 V or 0.05 V.[20] Accordingly, spectra for CO adsorbed at 0.4 V present a band for adsorbed water, exhibiting a constant frequency, which

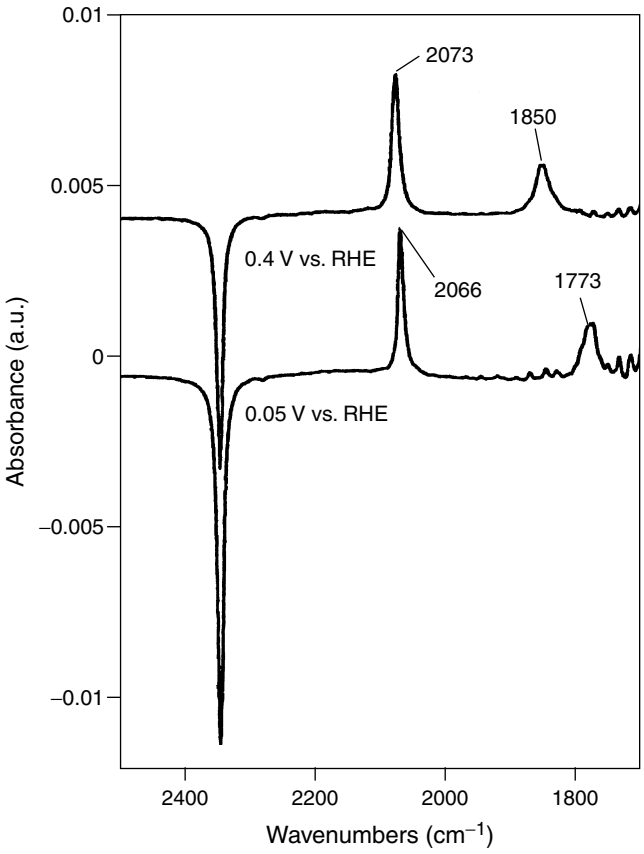

Figure 5. In situ FTIR spectra of the CO-adlayer formed on Pt(111) in CO-saturated 0.1 M $HClO_4$ solution at 0.05 V and 0.40 V vs. RHE as indicated in the spectra. See band assignment in the text. The reference spectrum was acquired after stepping to 0.8 V vs. RHE, the band for resulting CO_2 at 2341 cm^{-1} is also shown. (Reproduced from Villegas and Weaver (1994)[19] with permission from the American Institute of Physics.)

was interpreted as being due to an ice-like water layer which formed on top of the CO adlayer. The water overlayer acts as a blocking factor impeding CO oxidation[20] and shifts both overlayer transition and CO oxidation to higher potentials (0.65 V) than for CO adsorbed at 0.05 V. For the latter, no water bands were observed and in this case, the $(2 \times 2) \rightarrow (\sqrt{19} \times \sqrt{19})$ transition and the CO oxidation were observed at 0.4 V.[20] Furthermore, Yoshimi *et al.*[20] observed that the formation of the $\sqrt{19} \times \sqrt{19}$ structure begins at steps on the Pt surface. This observation agrees with the finding by Rodes *et al.* that the adlayer transition occurs at lower potentials for electrodes with a larger density of steps.[44] In view of the results discussed above, a rationalization of the activity of Pt(111) towards CO oxidation in the presence of bulk CO can be attempted. However, it must be taken into account that the enhancement of CO oxidation is not an exclusive property of Pt(111) (Figure 3).

Thus, it is likely that the increased current at low potential in the presence of dissolved CO, is due to a lowering of the adsorption energy for the saturated CO adlayer, as observed in the gas phase for different Pt surfaces.[36] While different Pt surfaces do present an increased activity for CO oxidation in CO-saturated solutions, the extent of reaction enhancement and the detailed current–potential behavior seems to depend on the Pt surface structure, as shown by Ackerman *et al.*[45] in a study of CO oxidation at Pt(111) and Pt(997), where the rate of oxidation and the state of the CO adlayer were simultaneously monitored by measuring the current and the second harmonic generation (SHG) signal from the surface.

The results of Yoshimi *et al.*[20] provide, at least for Pt(111), an explanation for the dependence of the activity for (bulk) CO oxidation on the admission potential: at admission potentials near 0.4 V vs. RHE an ice-like water structure is formed on top of the CO overlayer, which has a blocking effect and inhibits CO oxidation. While this explanation may be valid for Pt(111), we do not know, at present, whether an equivalent effect occurs on other surfaces. Other points remain unclear because of insufficient experimental documentation:

1. Which is the process responsible for the falling activity after the first potential scan?
2. More data on the dynamics and reversibility of the overlayer transitions are needed.
3. The fundamental unknown point is probably the question of the mechanism of reaction in the CO-saturated solution: how does the reaction between the CO molecules and water take place on a surface completely saturated with CO? Are holes eventually formed in the CO structure, sufficient for producing water dissociation at the rates observed at low potentials?

Understanding these processes at a molecular level will help to explain the intriguing catalytic behavior of CO at electrochemical interfaces.

2.3 Catalysis of CO oxidation by binary catalysts

In this section we consider catalyst promoters other than those adsorbing oxygen at low potentials as for example Ru. The latter are discussed in **The hydrogen electrode reaction and the electrooxidation of CO and H_2/CO mixtures on well-characterized Pt and Pt-bimetallic surfaces**, Volume 2.

Binder *et al.*[46] were the first to demonstrate that adsorbed sulfur on Raney Pt catalyzes the oxidation of bulk-carbon monoxide. As shown in Figure 6, the current for CO oxidation strongly increases in the presence of

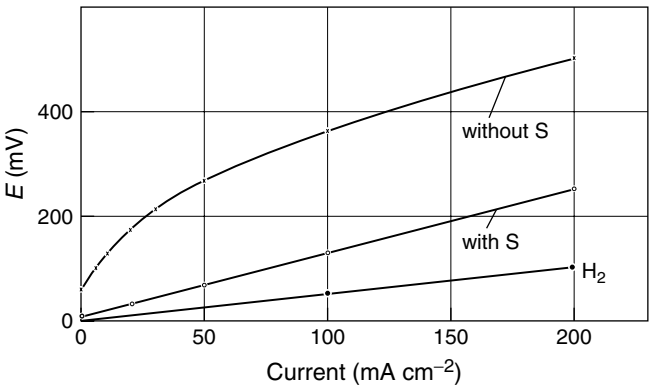

Figure 6. Stationary current–potential curves for CO in 1.5 M H_2SO_4, at 90 °C using Raney-platinum without and with S-coverage. Gas was continuously bubbled in the solution. For comparison data for H_2 oxidation are shown (both curves, with and without S fall together). (From Binder *et al.* (1967)[46] with permission from the authors.)

adsorbed S (S was deposited by applying a cathodic current (−500 mA) in warm 5 M H_2SO_4,[46] enhancement factor 6.3 by 200 mV). Interestingly, hydrogen oxidation (also shown in Figure 6) is not disturbed by the presence of adsorbed S atoms. Shibata and Motoo[47] studied the effect of several adatoms (S, Se, Te, Bi, Hg) on the rate of bulk CO oxidation at Pt. Figure 7 compares the currents measured at 450 mV for different adatoms. The catalytic effect clearly depends on the electronegativity of the adsorbed metal, increasing in the order Te < Se < S.

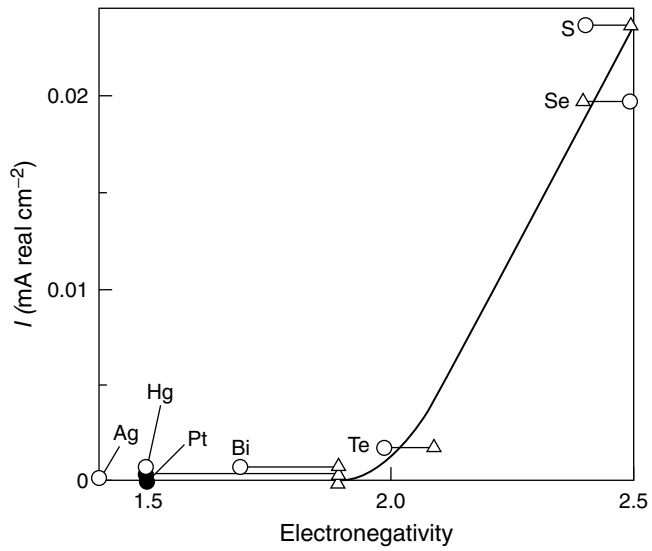

Figure 7. Dependence of the maximum current density for CO oxidation at 0.45 V in 0.5 M H_2SO_4 on the electronegativity of adatom. Electronegativity values from Pauling's (△) and from Alfred Rochow (○). (Reproduced from Shibata and Motoo (1985)[47] by permission from Elsevier Science.)

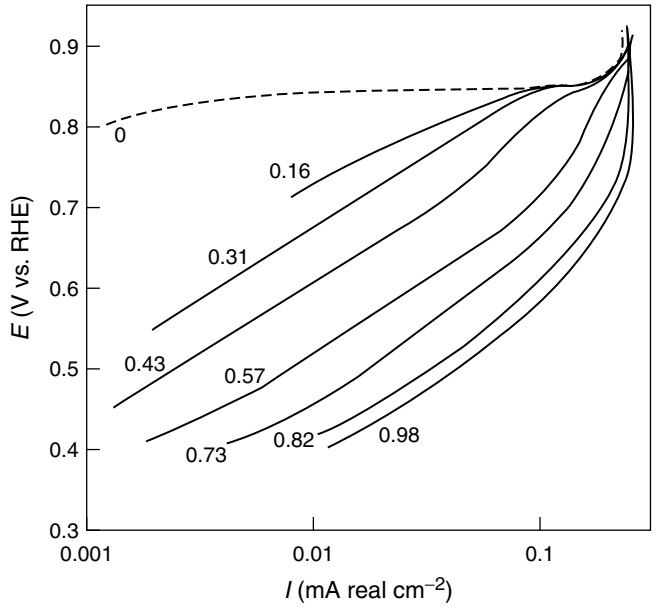

Figure 8. Semi-logarithmic plot of potential–current curves for CO oxidation on S-covered Pt electrodes in CO-saturated 0.5 M H_2SO_4 solution at 40 °C. Values of coverage θ_S^{Pt} for each curve are indicated. (Reproduced from Shibata and Motoo (1985)[47] by permission from Elsevier Science.)

Figure 8 shows curves for CO oxidation in the presence of different degrees of coverage by S. It is quite surprising that the current continuously increases with increasing coverage by S, this effect passing through a maximum at $\theta_S = 0.88$, $\theta_{Se} = 0.90$ and $\theta_{Te} = 0.65$. Degrees of coverage were calculated as:[48]

$$\Theta_M^{Pt} = \frac{{}_S Q_H - Q_H}{{}_S Q_H} \qquad (3)$$

where ${}_S Q_H$ and Q_H stand for the quantity of charge required to oxidize hydrogen adsorbed at 0.05 V on clean and adatom covered Pt, respectively.

It is currently accepted that CO oxidation can be enhanced in the presence of surface species adsorbing oxygen at low potentials (see below). However, none of the adsorbed atoms discussed here (S, Se, Te) exhibit this property.[49] Some approximation to the rationale for the catalytic effect of electronegative atoms can be gained by analyzing data for TPD of CO adsorbed on polycrystalline Pt pre-covered with S atoms.[49] It was observed that the temperature for CO desorption continuously decreases with increasing S coverage. The experiments were performed up to S saturation coverage (which allows a maximum adsorption capacity for CO, $\theta_{CO(max)} = 0.091$). This value is comparable with the one reported above for catalysis in the electrochemical cell. The phenomenon was interpreted in terms of a decrease of the binding energy of CO to the Pt surface, from 143 kJ mol^{-1} (for pure Pt) to 115 kJ mol^{-1} (for the S-saturated layer). It was suggested that this effect is due to a reduction of the capability of CO adsorption in the presence of sulfur: adsorption of CO causes a reduction of the density of electronic states within 3 eV of the Fermi level[49] and sulfur was found to interact with the band near 2.5 eV below the Fermi level.[50] Thus sulphur interacts with the local density of states at levels close to those normally used to bind CO. Weakening of the CO-metal bond is also invoked to explain the promoting effect of alloying Pt with some transition metals. According to Nørskov and co-workers,[51] the effect is produced by a lowering of the energy center of the d-band, which results in a diminished CO-metal binding energy.

Is the weakening of CO adsorption in the presence of sulfur the only reason for a sustained enhancement of CO oxidation at low potentials?

In principle, the same mechanism could be involved in catalysis by other electronegative atoms as Se and Te. The data in Figure 8 indicate an enhancement factor of ca. 10 for the current measured at 0.4 V at, say, 90% of S coverage. Thus, the effective enhancement factor is about 100, a result which is also valid for Se.[47]

The effect of these adatoms on the oxidation of bulk CO is completely different from that on the oxidation of adsorbed CO, i.e., when bulk-CO is absent. For the CO/Se *adsorbed* layers at Pt(111), Herrero *et al*.[52] suggested that well ordered mixed overlayers similar to those observed in UHV[53] are present in the electrochemical cell. They found an inhibition of CO stripping for Se and Te. Unfortunately, their data do not refer to oxidation in the presence of dissolved CO.

Thus, the question arises on the CO reaction mechanism for dissolved CO in the presence of these adatoms. Taking the data of desorption energy for CO at Pt(111)/S (115 kJ mol^{-1}), we conclude that CO is still very stable on this surface and all adatom-free Pt sites should become covered with CO. It seems unlikely, that in the presence of dissolved CO, an additional lowering of the adsorption energy occurs as suggested before for the pure metal, since repulsion between CO neighbors should be less effective in the presence of a high coverage with adatoms. However, it cannot be discarded that a state of the type $CO(CO_{ad})$, involving loosely bonded CO molecules onto a strongly adsorbed CO layer exists, as suggested by Ertl and co-workers for saturated CO allayers in the gas phase.[38] As these authors suggested, such states can involve very low CO desorption energies. Under conditions of high adatom coverage no available sites for water dissociation are expected and a Langmuir–Hinshelwood mechanism seems to be unlikely. A reaction via an Rideal–Eley mechanism between weakly bonded CO and water molecules

from the solution phase cannot be discarded. It has been argued, for heterogeneous reactions in the gas phase, that the probability of reaction via this mechanism is very low, because the residence time for a gaseous molecule impinging the surface is very low (ca. 1 ps). In addition, in UHV the impinging rate is also very low.[25] The situation in the electrochemical cell is quite different since the reaction partner, water, has a concentration of 55.5 mol l^{-1} and bombardment of the surface by water molecules should be much more effective than in the gas phase. Obviously, a definitive answer to this question requires a lot of new experimental effort.

3 METHANOL ELECTROOXIDATION

3.1 General features

The thermodynamic standard equilibrium potential for complete oxidation of methanol to CO_2 is $E^\circ = 0.02$ V (see Table 1). However, as shown in Figure 1 for a platinum electrode, under conditions of current flow, kinetic inhibition strongly shifts the potential by several hundreds of millivolts. Additionally the total oxidation,

$$CH_3OH + H_2O \longrightarrow CO_2 + 6H^+ + 6e^- \qquad (4)$$

delivering 6 electrons per mol of methanol, can be accompanied by the formation of by-products following parallel reactions as early suggested by Breiter.[5] In a simplified manner the reactions can be written as follows:

$$CH_3OH \longrightarrow \text{(adsorbed intermediates)} \begin{cases} \nearrow\ CO_{ad} \longrightarrow CO_2 \\ \searrow\ HCHO,\ HCOOH \longrightarrow CO_2 \end{cases} \qquad (5)$$

This formulation may be critical in the sense that it is not known at present to what extent formaldehyde and formic acid should be considered reaction intermediates and/or reaction by-products. It is well known that both these substances can also form adsorbed CO at Pt surfaces and that formic acid itself undergoes a dual pathway oxidation to CO_2.

A catalyst for methanol oxidation should be able to (a) dissociate the C–H bond and (b) facilitate the reaction of the resulting residue with some O-containing species to form CO_2. On a pure Pt electrode, which is known to be a good catalyst for breaking the C–H bond, the two processes necessary for complete oxidation occur in different potential regions:

- Process (a) involving the adsorption of methanol molecules, requires several neighboring places at the surface and, due to the fact that methanol is not able to displace adsorbed H atoms, adsorption can only begin at potentials where enough Pt sites become free from H, i.e., near 0.2 V vs. RHE for a polycrystalline Pt electrode.
- The second process (b) requires dissociation of water, which is the oxygen donor of the reaction. On pure Pt electrode, sufficient interaction of water with the catalyst surface is only possible at potentials above 0.4–0.45 V vs. RHE.[54, 55]

Thus, on pure Pt, methanol oxidation to CO_2 cannot begin below, say 0.45 V. However, the adsorbate layer does not exhibit a good reactivity below at least 0.7 V, i.e., at potentials without technological interest.

3.2 Methanol adsorption

It was suggested that methanol adsorption takes place in several steps, forming different species due to dissociation of the molecule:[6]

$$CH_3OH \longrightarrow \underset{x}{CH_2OH} + H^+ + e^- \qquad (6)$$

$$\underset{x}{CH_2OH} \longrightarrow \underset{xx}{CHOH} + H^+ + e^- \qquad (7)$$

$$\underset{xx}{CHOH} \longrightarrow \underset{xxx}{COH} + H^+ + e^- \qquad (8)$$

$$\underset{xxx}{COH} \longrightarrow \underset{x}{CO} + H^+ + e^- \qquad (9)$$

where x stands for a (formerly water covered)[54] Pt site. It was also suggested that formaldehyde and formic acid could be formed from the intermediates CH_2OH and CHOH, respectively.[6]

If a cyclic voltammogram is started after contacting a polycrystalline Pt electrode with a methanol-containing solution at a potential of 0.05 V or less, methanol adsorption can be observed as soon as hydrogen coverage decreases to a certain extent. The dissociation process gives rise to a current peak in the H-region (Figure 9), which can be observed only during the first potential scan, i.e., when the surface is free from organic residues. The experiment in this figure was performed using the DEMS technique (**Product analysis**, Volume 2).[13] Briefly, in this technique the electrode is a porous Pt layer on a PTFE membrane, sitting at the entrance of a mass spectrometer (MS). This setup allows the on-line detection of volatile products entering the MS within fractions of a second after being formed. As illustrated in Figure 9 no signal for mass (m/e = 44) corresponding to CO_2 was detected at potentials in the region of the current peak. No other volatile products were detected and it can be concluded that the current peak

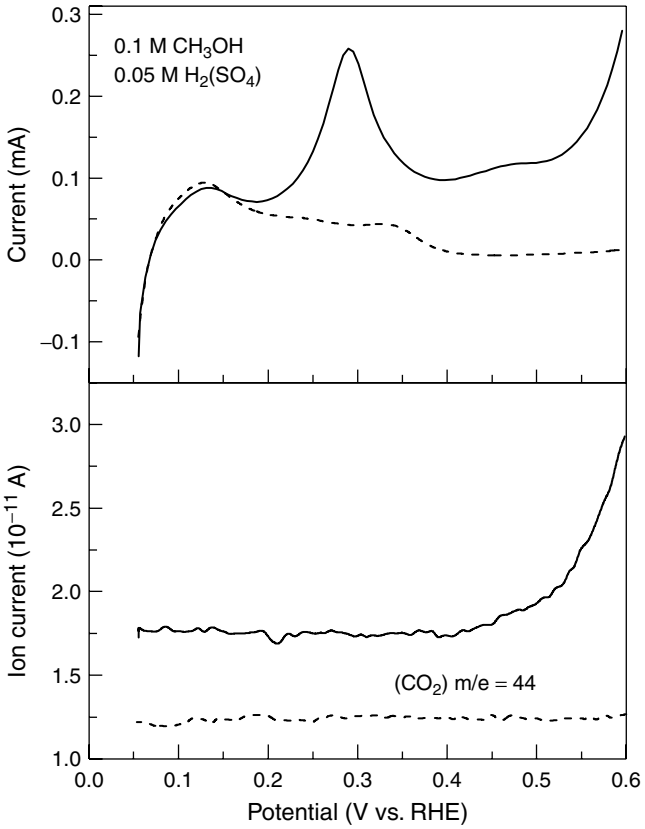

Figure 9. First current and mass-signal voltammograms during the methanol adsorption and oxidation. The electrode, a porous polycrystalline Pt was contacted with the methanol solution at 0.05 V, 0.1 M CH_3OH/1 M $HClO_4$; 20 mV s^{-1}. Surface roughness: ca. 50.

is related to faradaic processes occurring during methanol adsorption.

3.3 The nature of the adsorbed methanol species

Establishing the nature of adsorbed species formed during adsorption of small organic molecules is a difficult task. The issue was approached in the past in a number of studies using pure electrochemical methods.[2] Except from a study using gas chromatography[5] earlier papers were mainly based on data of charge measurements during adsorption of methanol and oxidation of the adsorbed residue.[2, 4, 18] The use of analytical methods for the in situ, ex situ and online analysis of the electrode surface began in the 1980s.[11] Different adsorbed species were suggested on the basis of data from infrared spectroscopy,[11, 12, 56] thermal-desorption MS[11, 57] and DEMS.[11]

Infrared spectra obtained during methanol adsorption at 0.35 V on polycrystalline Pt show well-characterized bands for linearly bonded CO at ca. 2040 cm^{-1} together with other bands in the 1200–1300 cm^{-1} region, which have been interpreted in terms of the C–OH stretching of hydrogenated species (as, e.g., COH[56] or HCOH). These bands were also observed in spectra obtained on single crystal Pt(100) and Pt(111)[58] (see below).

Another approach to establish the nature of the adsorbate was made by thermal desorption mass spectrometry, performed on electrodes transferred into UHV.[57] These results confirmed the presence of hydrogenated species in the residues produced upon methanol adsorption. Moreover, these data have shown that the ratio between the amount of CO and other (hydrogenated) species depends on methanol concentration.[57] It should be noted that large discrepancies in the results from different groups may lie, at least in part, in differences in the experimental approach. The necessity to thoroughly eliminate traces of oxygen from the solution and from the gas atmosphere above the solution has been emphasized. Adsorbed oxygen can interact with organic residues; recall that O_2 reduction on a Pt surface produces adsorbed peroxide intermediates, which can act as oxidizing agents.

3.4 Methanol oxidation products

The oxidation products of CH_3OH are well known since the works of Pavela[59] and Schlatter.[60] These authors used long-term electrolysis at potentials between 0.5 and 0.6 V vs. RHE and found CO_2, H_2CO, HCOOH and $HCOOCH_3$. The product methyl formate originates in a reaction between HCOOH and CH_3OH:

$$HCOOH + CH_3OH = HCOOCH_3 + H_2O \qquad (10)$$

The yields of different products depend on methanol concentration, temperature, electrode roughness and time of electrolysis.[61, 62] Carbon dioxide formation was found to be favored at high temperature and on rough electrodes. Figure 10(a)[62] shows the time dependence of the amount of products formed on a platinized Pt electrode at a constant current of 50 mA (other details are given in the figure caption). From the slope of curves C the rate of product formation can be calculated. After ca. 50 h the current efficiency for CO_2 is about 95% and the efficiency for HCOOH and HCHO falls down to zero (Figure 10b). The results of Ota *et al.* for a platinized Pt electrode in 1 M CH_3OH + 1 M H_2SO_4, measured at 0.6 V are given in Table 2.[62]

The study of the products of methanol oxidation during a potential scan was the first goal of online mass spectrometry, DEMS.[13] In Figure 11, the potentiodynamic formation of CO_2 on a porous polycrystalline Pt electrode was followed during the potential scan by recording the

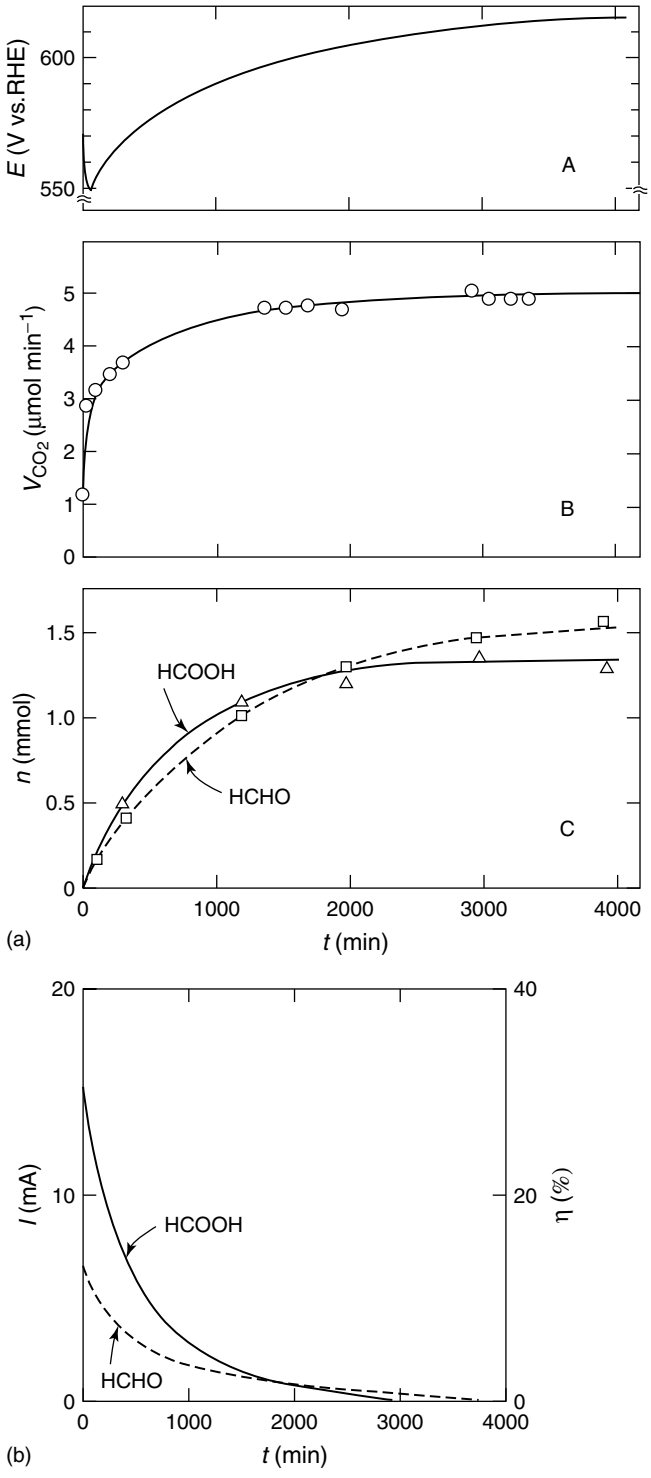

Figure 10. Soluble products of methanol oxidation. 1 M CH_3OH + 1 M H_2SO_4. Constant applied current, 50 mA; electrode, platinized Pt (roughness factor 690); temperature, 25 °C. (a) Time dependence of potential (A) and amount of soluble products (B) CO_2, (C) HCOH and HCOOH as indicated. (b) Reaction current and current efficiency for HCOOH and HCOH. (Reproduced from Ota *et al.* (1984)[62] with permission from Elsevier Science.)

Table 2. Current efficiencies of methanol oxidation in 1 M CH_3OH, 1 M H_2SO_4 after 50 min of electrolysis using platinized Pt electrodes of different roughness factors; 0.6 V vs. RHE, 25 °C.[62]

Roughness factor	Q_{total} (C^{-2})	Current efficiency (%)		
		CO_2	HCHO	HCOOH
102	31	25	53	22
282	135	44	31	25
696	388	63	12	25
970	613	69	7	24

ratio m/e = 44 for CO_2 and 60 for methyl formate. Another product, di-methoximethane ($CH_2(OCH_3)_2$), produced by the reaction of HCHO and CH_3OH gave a very weak signal for mass 75.[11] There must be some problem with the volatility of formaldehyde or its derivative product in aqueous solution (gem diol, $CH_2(OH)_2$), making difficulties with the direct detection via the DEMS technique.[63] On technical electrodes di-methoxi methane was detected by DEMS,[64] at high temperature (175 °C). In this case the yields were dependent on the amount of water in the gaseous methanol/water mixture used (see **Product analysis**, Volume 2). These difficulties extend to other modern analytical methods such as in situ FTIR as pointed out by Korzeniewski and Childers.[65] This could be the reason why formaldehyde remained almost disregarded in the methanol fuel cell literature. In fact, when methanol in acid solution is brought into contact with a platinum electrode, formaldehyde is formed already at open circuit.[66] Korzeniewski and Childers determined formaldehyde yields fluorometrically, after applying a constant potential to a smooth polycrystalline Pt electrode during 5 min in a micro cell. Their results show 38% of formaldehyde at 0.25 V vs. (saturated) Ag/AgCl in 15 mM CH_3OH + 0.1 M $HClO_4$ solutions, the yield decaying at higher potentials. Thus, e.g., at 0.45 V vs. Ag/AgCl, the main reaction product is CO_2 (80%), and the yield of HCOH fell to only 8%.[65] On the other hand, much higher amounts of formaldehyde are reported by Wang *et al.*[63] for porous Pt in 10 mM CH_3OH + 0.5 M H_2SO_4. According to these authors, 50% HCOH is obtained at 0.65 V vs. RHE and no differences were observed when using 0.1 M $HClO_4$ as a supporting electrolyte. It must be noted that formaldehyde data of Wang *et al.* were not directly measured but calculated from the amounts of CO_2 and HCOOH via DEMS (under the given conditions, the reported yields of HCOOH and CO_2 were 34% and 16%, respectively[63]) and comparing these values with the total charge passed. However, the results of Wang *et al.* can be compared with those of Ota *et al.* for rough electrodes in 1 M CH_3OH (Table 2), but cautiously, since the latter refer to a much higher methanol concentration.

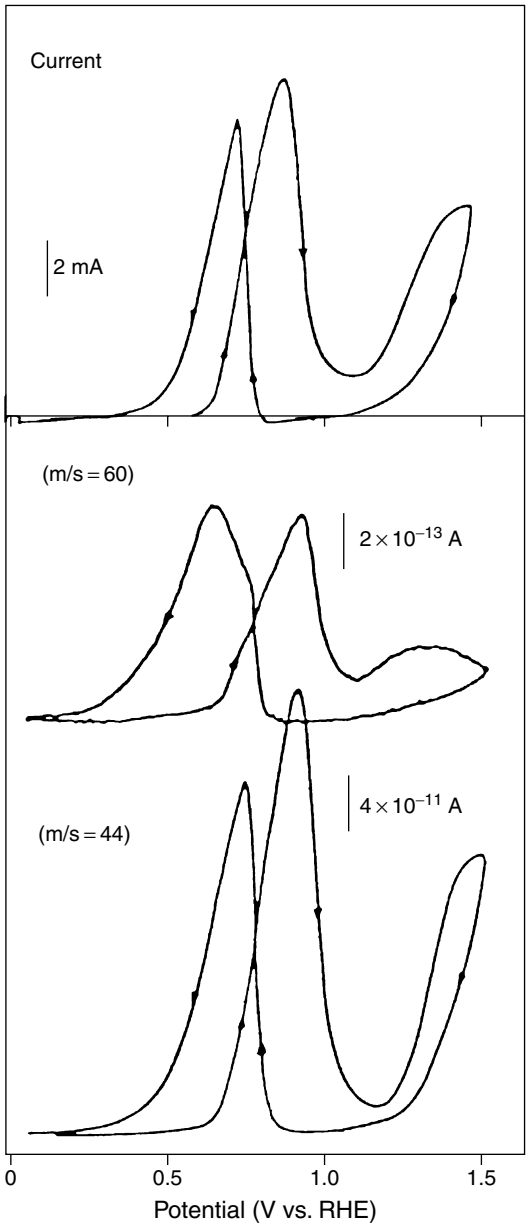

Figure 11. DEMS experiment: current and mass-signal (m/e = 44, CO_2 and m/e = 60, methyl formate) voltammograms during methanol oxidation on a porous Pt electrode. 0.1 M CH_3OH/1 M $HClO_4$; 20 mV s^{-1}. Surface roughness: ca. 50. (Reproduced from Iwasita (1990)[11] with permission from VCH.)

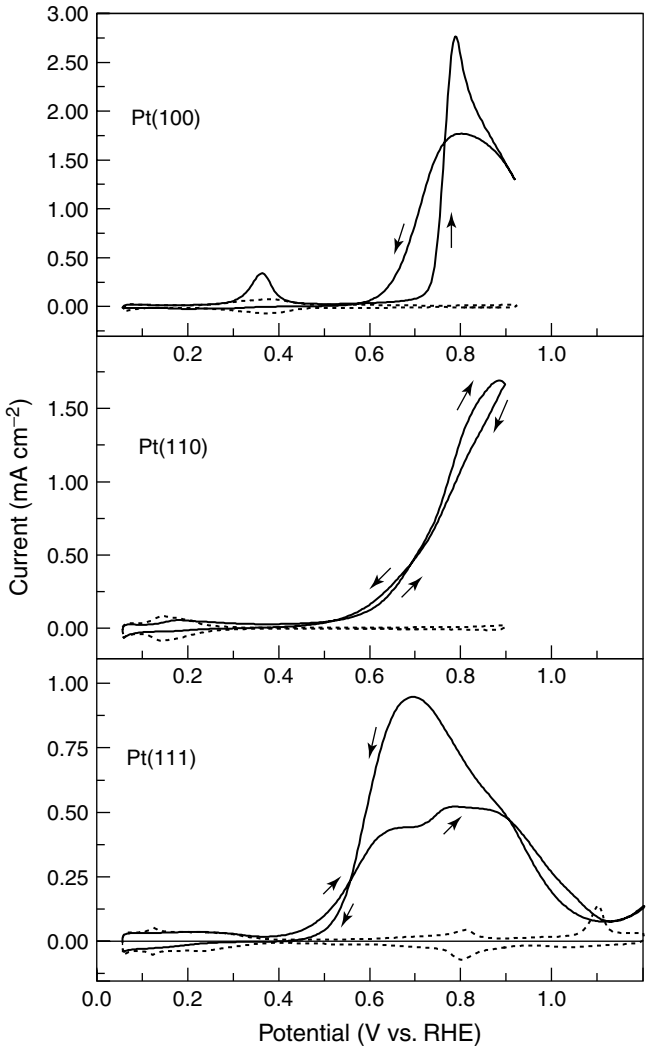

Figure 12. First potential scan for methanol oxidation on Pt(hkl). 1.0 M CH_3OH in 1.0 M $HClO_4$; sweep rate = 50 mV s^{-1}. (Reproduced from Xia *et al.* (1996)[58] with permission from Elsevier Science.)

3.5 Structural dependence of methanol oxidation

3.5.1 Results of cyclic voltammetry

The complexities involved in methanol adsorption and oxidation are reflected in the strong sensitivity of the reaction to the surface structure. Cyclic voltammograms of methanol on the three low index surfaces of monocrystalline platinum in 0.1 M $HClO_4$ are shown in Figure 12.[58] The Pt surfaces in these experiments were contacted with methanol at 0.05 V (a potential where methanol adsorption is negligible) and then the first scan of the cyclic potential sweep was recorded at 50 mV s^{-1}. From the three surfaces, Pt(100) is the only one presenting a well-defined curve for methanol dissociative adsorption. This process is observed as a well-defined peak at 0.35 V, superimposed on the current for H-desorption (see also Figure 9). The adsorption process at Pt(100) causes the blocking of the electrode surface. Therefore, almost no activity toward oxidation is observed until the potential reaches ca. 0.72 V. Contrasting with this result, no indication of dissociative adsorption or blocking of the surface is observed at Pt(111). At Pt(110) one observes a lower current in the H region, which may indicate that the surface is partially blocked already at the beginning of the potential sweep. This behavior is not

surprising in view of the low potential for H desorption on this surface. For a comparison, the first part of the potential scan is magnified in Figure 13. Here, one sees that a CV for Pt(111) shows up the highest oxidation current between 0.45 and 0.65 V, followed by Pt(110) and Pt(100). However, before establishing a ranking for the activity of the three surfaces, infrared results should be taken into consideration, as we shall do in the next section.

So far we have discussed results obtained in $HClO_4$ as a supporting electrolyte. The nature of the anions present in solution may have an effect on the rate of reaction. In particular, specifically adsorbed anions can act as a barrier for methanol adsorption. This issue has been studied using cyclic voltammetry.[67, 68] Particularly important is the comparison of results obtained with $HClO_4$ and H_2SO_4, two electrolytes currently used in electrocatalysis studies. Whilst it is accepted that perchlorate ions are not specifically adsorbed at Pt, adsorption of sulfate species has been well established via in situ FTIR spectroscopy.[14, 69, 70] Judging from the intensity of infrared bands for adsorbed sulfate, adsorption is stronger on Pt(111) than on Pt(100). This is also supported by the fact that adsorption of sulfate species causes the current under the so-called *unusual states*[15] in the voltammogram of Pt(111) between ca. 0.35 V and 0.5 V in 0.5 M H_2SO_4. This peculiar behavior indicates a strong interaction of the adsorbed anion with the Pt(111) surface and, therefore, one additional aspect to be considered here is how the supporting electrolyte affects methanol oxidation. This problem was approached by comparing the cyclic voltammogram responses in $HClO_4$ and H_2SO_4.[67, 68] In Figure 14 the first sweep during methanol oxidation on Pt(111) in both supporting electrolytes is shown. Much larger currents (a factor of 10) are observed in $HClO_4$ than in H_2SO_4. This effect seems to be caused by the strong specific adsorption of the anion in H_2SO_4. Identical results as in Figure 14 were reported by Kita *et al.*[68] who also observed higher currents in $HClO_4$ for Pt(100) (factor of two) while no difference between $HClO_4$ and H_2SO_4, was observed at Pt(110).[68]

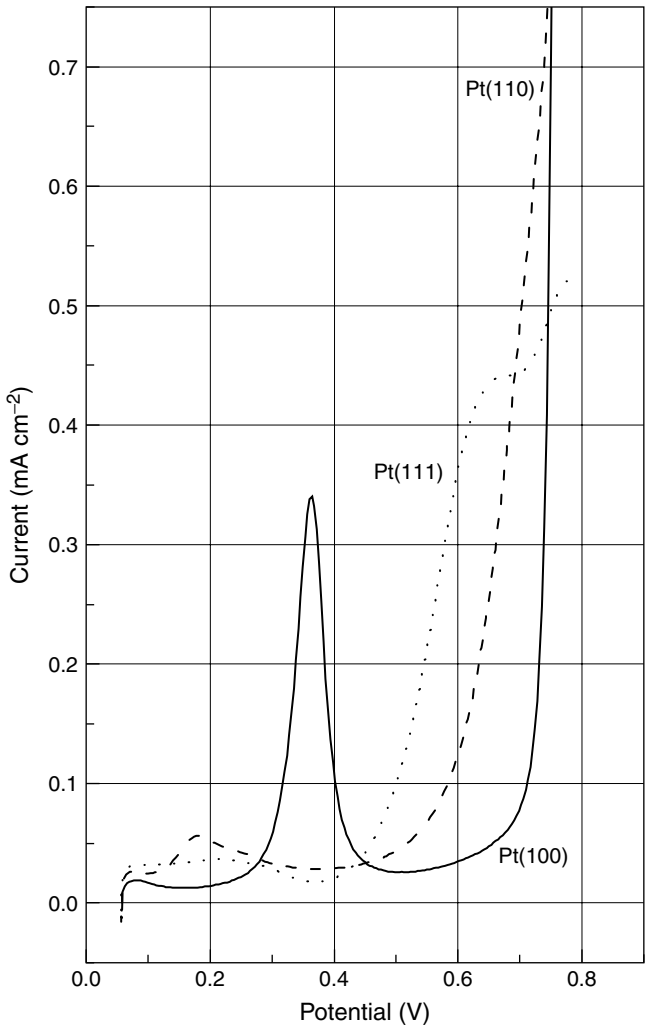

Figure 13. Comparison of the current during a potentiodynamic scan in 1.0 M CH_3OH + 1.0 M $HClO_4$ on Pt(hkl); sweep rate = 50 mV s^{-1}.[58]

3.5.2 *Results of infrared spectroscopy*

Infrared spectra during methanol adsorption and oxidation are shown in Figure 15, for Pt(111) Pt(100) and Pt(110)[58] in 1 M CH_3OH solutions, using 0.1 M $HClO_4$ as supporting electrolyte. Bands at ca. 2060 cm^{-1} and 1850 cm^{-1} are assigned to linearly (CO_L) and bridge (CO_B) bonded CO,

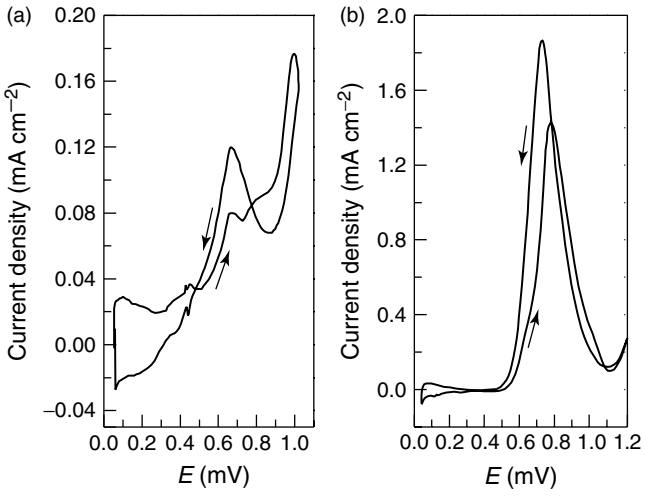

Figure 14. Potentiodynamic curves for methanol oxidation on a Pt(111) electrode in 1.0 M CH_3OH solution with (a) 0.5 M H_2SO_4 and (b) 0.1 M $HClO_4$ supporting electrolytes. Sweep rate: 20 mV s^{-1}.

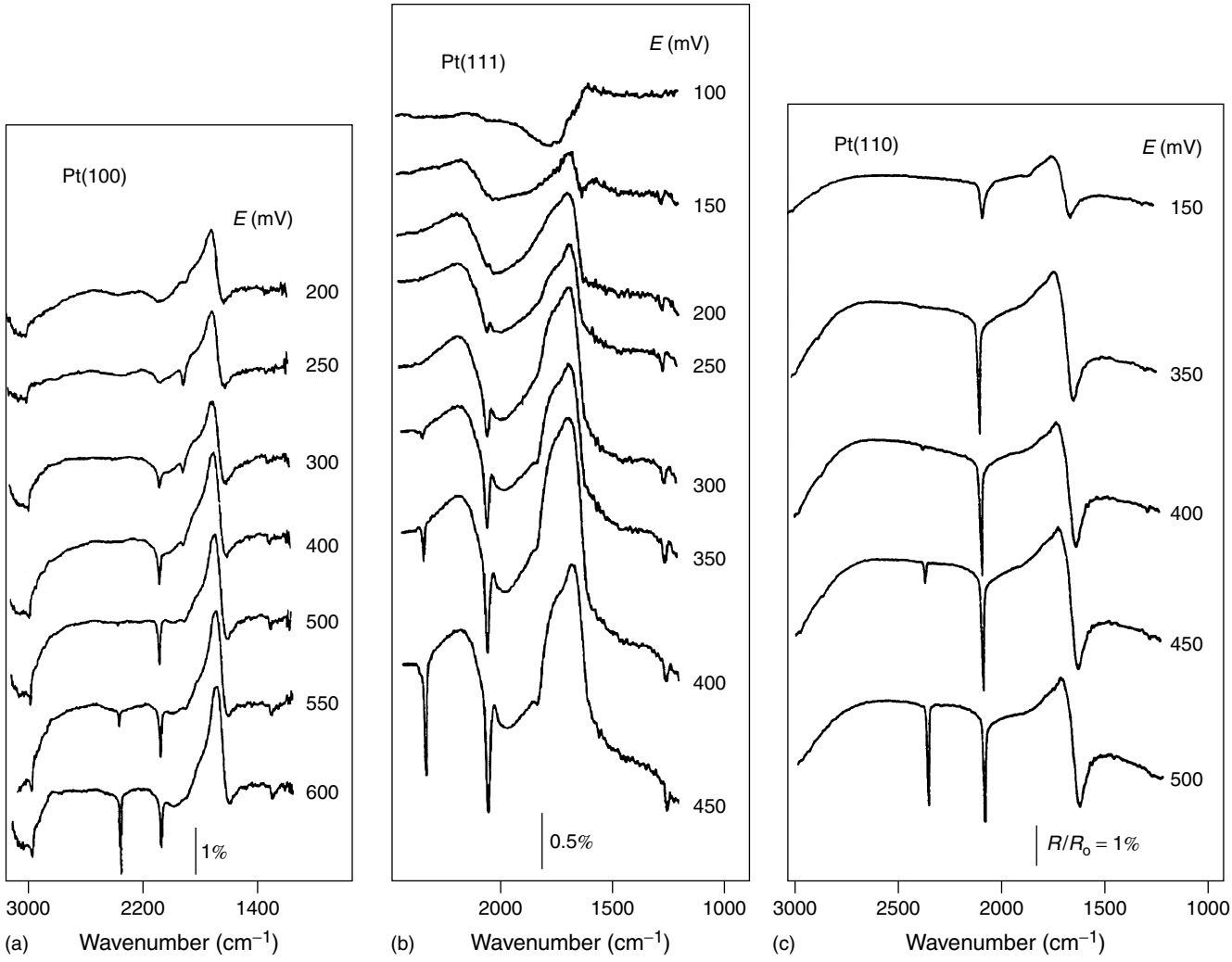

Figure 15. Infrared spectra in 1.0 M CH_3OH in 0.1 M $HClO_4$ at Pt(100) (a), Pt(111) (b) and Pt(110) (c). Reference spectra collected at 50 mV; sample spectra collected at the indicated potentials.[58]

respectively. The band at 1260 cm^{-1} was assigned to some H-containing intermediate, possibly COH[56] and the band at 2341 cm^{-1}, observed on all spectra, is due to CO_2. Other H-containing adsorbate may be responsible for the feature at 2950 cm^{-1} in the spectra for Pt(100). This band, appearing already at 0.2 V and becoming better defined at more positive potentials can be assigned to the C–H stretching of a CH_2 group in an adsorbed species. All spectra develop a band at 2341 cm^{-1}, as the product CO_2 is formed. Although not shown here, a weak band at 1230 cm^{-1} has been observed at Pt(111) from ca. 0.55 V onwards, which was assigned to the C–O–C stretching of methyl formate.[58]

The surface sensitivity of the reaction can be also analyzed in a plot of the integrated band intensities for CO and CO_2 for different monocrystalline surfaces as shown in Figure 16(a,b). In comparing these results with those of cyclic voltammograms (CVs), one has to be aware that the time scale for the spectra is larger than for the CV. Thus, the voltammetric curves in Figure 13 were taken at 50 mV s^{-1}, i.e., 0.02 s mV^{-1}. On the other hand, spectra collection requires about 70 s at each potential and considerable adsorption can take place during this time.

The behavior of Pt(111) and Pt(110) highlights some interesting features of the mechanism of methanol oxidation. We will leave Pt(100) out of consideration at first because this surface presents two forms of adsorbed CO (ontop and bridge), thus disabling coverage estimations on the basis of the band intensity.[21] In the case of Pt(111) the intensity of the band for CO_B is so small that we shall simply neglect it in the following discussion.

Measurable amounts of CO have already been observed at Pt(110) at 0.1 V. The CO feature rapidly grows with

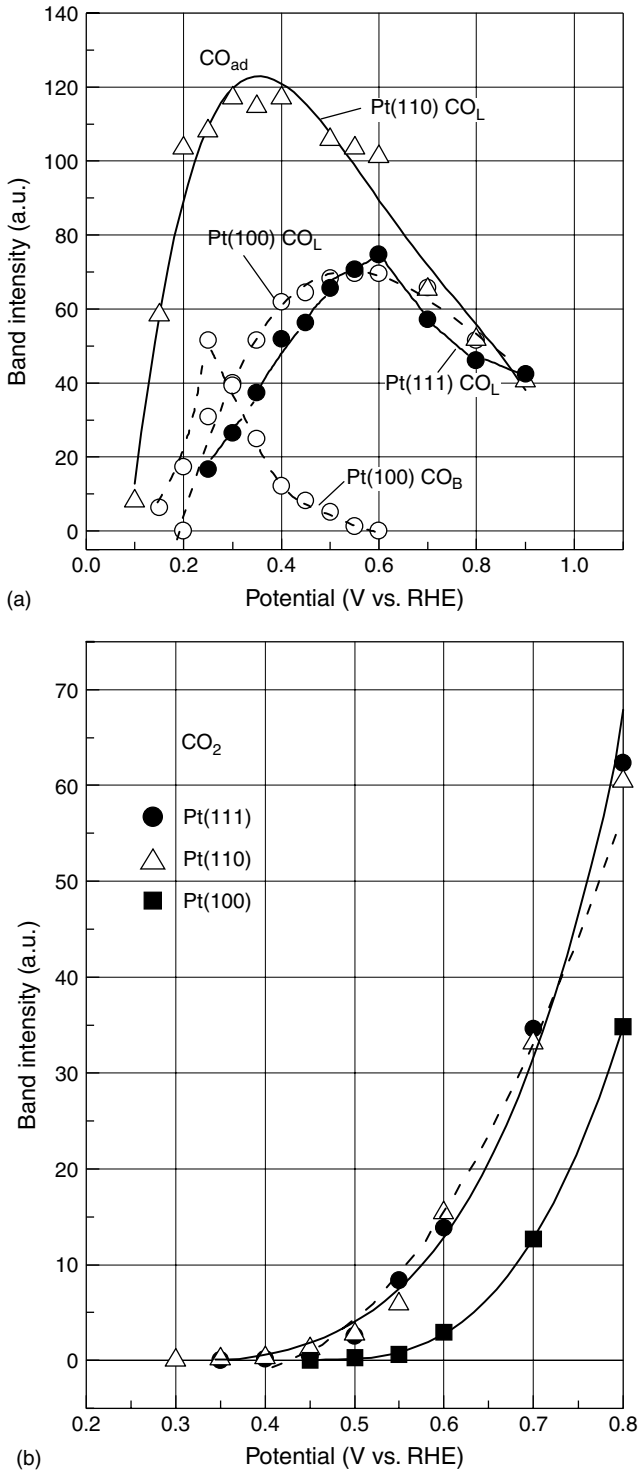

Figure 16. Integrated band intensities from IR spectra at Pt(111) and Pt(100) and Pt(110) in 1.0 M CH_3OH in 0.1 M $HClO_4$. (a) linear (CO_L) and bridge (CO_B) bonded carbon monoxide; (b) CO_2.

potential and already reaches a maximum at 0.3 V. At Pt(111), a band for linear bonded CO can be seen, the intensity of which grows somewhat more slowly than that for Pt(110). The initial adsorption can be extrapolated to around 0.2 V. But the most important observation here is that the dissociative adsorption of methanol at Pt(111) takes place at potentials within the H region. Therefore we can conclude that the lack of adsorption in the H-region during the potential scan at 50 mV s^{-1} (Figure 13) can be explained as due to a large kinetic limitation in the adsorption process at Pt(111) which is not observed on the other two surfaces (see discussion below).

In Figure 16(b) the integrated band intensity for the CO_2 observed in the potential region below 0.8 V is presented. We can state that in this region CO_2 production proceeds with almost the same rate at both Pt(111) and Pt(110) and is much slower at Pt(100). Both former surfaces have almost the same catalytic activity for CO_2 production, at least at potentials below ca. 0.7–0.75 V. However, the relative currents observed in Figure 13 for Pt(110) and Pt(111) indicate a higher activity of the latter towards methanol oxidation. This apparent contradiction indicates that in the interval of potentials between, say, 0.4 and 0.6 V, the potentiodynamic current at Pt(111), originates to a large extent from the process of adsorbing methanol and/or from the parallel pathway forming HCOOH and/or HCHO. Our present knowledge of the yields of HCOOH and/or HCHO at single-crystal electrodes is insufficient for establishing the extent to which these pathways contributes to the current. Pt(100) also presents evidences for high yields of the parallel reaction: the pronounced increase of current at 0.7 V (Figure 13) contrasts with the moderate variation of the CO_2 band intensity in Figure 16(b).

3.6 The mechanism of methanol oxidation

Understanding the mechanism of methanol oxidation is an issue which can be considered to be in its infancy. The slow progress over many years can be easily understood in the light of the difficulties created by the existence of parallel reaction paths with yields depending on potential, time, surface structure, etc. At present, we can only distinguish the two global processes already indicated in the introduction namely, *adsorption* of methanol molecules and *oxidation* of adsorbed residues. The IR results will help us to follow the potential dependence of the pathway leading to CO_2 via formation of adsorbed CO and identify, for this pathway, whether adsorption of methanol or removal of CO is the rate-determining process.

Due to the fact that the interface components of the respective Pt surfaces depend on potential and considering the necessity of some adsorbed oxygen donor, for oxidation of the adsorbed residues, we can state that both these effects

can only take place simultaneously at potentials above 0.4 V or higher. However, with respect to the adsorption process, we should start the discussion by considering methanol adsorption at potentials below 0.4 V. It is well known that methanol cannot displace adsorbed hydrogen from the Pt surface. This is a well known phenomenon and is documented by the data in Figure 16(a). We follow here the discussion on the structural dependence of methanol adsorption started in the previous section, by recalling that data were obtained by applying potential steps of ca. 70 s of duration and therefore are neither stationary nor dynamic. However, the procedure for collecting spectra was the same for all surfaces and a comparison of the band intensities can give an idea of the rate of methanol adsorption in the low potential region. Thus, adsorption of methanol occurs at a higher rate at Pt(110) than at Pt(111) (Figure 16a). While CO_L coverage at Pt(110) rapidly increases reaching a saturation value between 0.3 V and 0.4 V, the band for CO_L at Pt(111) grows more slowly and does not present a real maximum but a sudden falling of intensity at a potential of 0.6 V. Additionally, in the whole range of potentials the CO band intensity is substantially higher on Pt(110) than on Pt(111). More about the methanol adsorption process can be learnt by analyzing in parallel the band intensity for CO in Figure 16(a) and the hydrogen coverage according to the voltammograms of these surfaces measured in $HClO_4$ (Figure 17). Thus, e.g., for Pt(110) at 0.2 V vs. RHE, $\theta_H \sim 0.2$; at this potential the band intensity for CO is quite large (about 80% of its maximum value). On the other hand, for the same θ_H at Pt(111) ($E \sim 0.29$ V), the band intensity is much lower and slowly grows with increasing potentials even beyond 0.4 V, where the surface is free from adsorbed hydrogen. It can thus be concluded that the difference in methanol adsorption rate for these two surfaces originates in some property inherent to the surface itself and not in the amount of sites free from adsorbed hydrogen at a given potential.

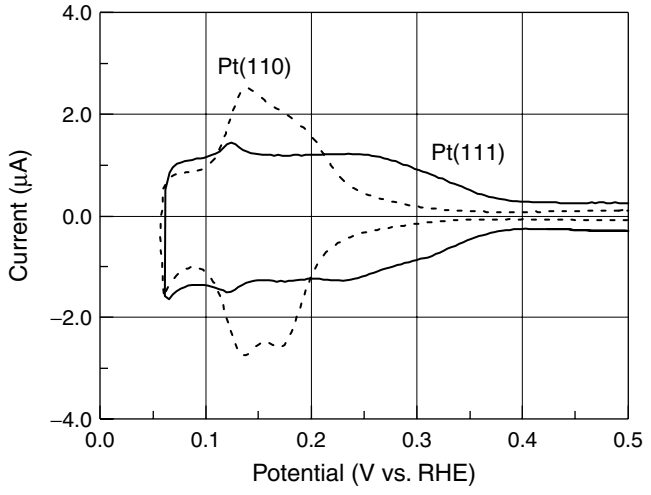

Figure 17. Potentiodynamic current-potential response between 0.05 and 0.5 V vs. RHE for Pt(111) and Pt(100) in 0.1 M $HClO_4$; sweep rate 50 mV s^{-1}.

We now consider the potential region above 0.4 V, where CO_2 is produced. Independently of the respective CO coverage, the rate of CO_2 formation is the same for both surfaces Pt(111) and Pt(110) and hence, they present identical rates of the corresponding pathway. The most simple interpretation of this result is that the rate determining process is the oxidation of the residue adsorbed. Or, in other words, in the range of potentials analyzed here (ca. 0.4–0.7 V), there is enough adsorbed methanol on both surfaces to reach the maximum rate for the production of CO_2. Gasteiger *et al.*[71] suggested that oxidative removal of CO is the rate-determining-step (rds) in this potential region. Following a somewhat different approach, Christensen *et al.*[72] arrived at the same conclusion for polycrystalline Pt. Summarizing, oxidation of adsorbed CO and not adsorption of methanol is likely to be the rate-determining process in the potential region between, say, 0.4 and 0.70 V.

At higher potentials, interaction of water with the Pt surface increases[54] and competition of methanol with water for adsorption sites becomes important.[55] Therefore, at potentials above, say, 0.7 V, methanol adsorption becomes the rds again and in this region the reaction rate passes through a maximum and then decays.

For the pathway analyzed here, leading to CO_2 formation via adsorbed CO, we can state that CO is an intermediate of the reaction and the role of surface poison usually ascribed to CO_{ad} should be revised. Inspection of Figure 16(a) indicates that CO indeed accumulates on the surface at low potentials (see the result for Pt(110)), however, the reason for the lack of CO_2 formation lies in the inability of Pt to dissociate water and not in the degree of surface blocking by CO. Otherwise it would be difficult to understand how two surfaces covered with CO to different extents produce CO_2 at identical rates.

Concerning the nature of the oxygen donor there has been a more or less general consensus that it is an adsorbed OH species coming from water dissociation, as originally suggested by Gilman.[37] According to Wieckowski *et al.*[73] the oxygen donor is simply some activated water molecules adsorbed on the Pt surface. However, for oxidative stripping of CO adlayers on platinum, Koper *et al.*[39] have shown that the dissociation of water is a necessary step in order to harmonize experimental data with the results of Monte Carlo simulations.

3.7 Catalyst promoters for methanol oxidation

Several binary and ternary catalysts have been proposed for methanol oxidation, most of them based on modifications of Pt with some other metal. The promoter metal must fulfill the requirement of forming O-containing surface species at low potentials. This seems to be *sine qua non* for increasing the catalytic activity of Pt towards methanol oxidation. Among others, Sn,[7–9, 74] Bi,[75] Mo[76] and Ru[7, 77–94] were suggested. There are, of course, several practical factors limiting the choice of the metal. Many O-adsorbing metals can produce negative effects, e.g., inhibit methanol adsorption or may be not sufficiently stable for long-term use, as required for a fuel cell. At present, there is a general consensus that PtRu offers the most promising results. The catalytic effect has been observed in different kinds of PtRu materials, such as PtRu alloys,[77, 79, 83–85, 89–91, 94] PtRu electrodeposits,[82] Ru evaporated on Pt,[85] Ru adsorbed on single-crystal Pt(hkl),[85–88] and on technical (carbon supported electrodes) as well.[90, 91]

When discussing the reason for the enhanced rate of methanol oxidation on PtRu, the *bi-functional* mechanism is often invoked.[78] The term was suggested to give emphasis in the joint activities of both metals, Pt being the one adsorbing and dissociating methanol and Ru, the one oxidizing the adsorbed residues. This description of the mechanism is based in the observation that at potentials below 0.4 V, Pt is a good catalyst for methanol adsorption, but not for water dissociation while Ru is able to dissociate water but it cannot adsorb methanol. However, establishing a role for each metal as in the bi-functional mechanism is of limited use, since it is well known that at high potentials Pt dissociates water and, as shown in Refs. [84, 94] at high temperatures (60–80 °C) Ru adsorbs methanol. Moreover, even for conditions where methanol adsorption occurs only on Pt, CO can move on the surface and occupy sites on Ru atoms. Altogether, several adsorbed species could be involved in the oxidation process at the PtRu catalyst, namely, $Pt(CO)_{ad}$, $Ru(CO)_{ad}$, $Ru(OH)_{ad}$ and $Pt(OH)_{ad}$. To simplify, we can describe the bi-functional mechanism as follows.[71]

The first step of the reaction is adsorption of methanol:

$$CH_3OH_{(sol)} \longrightarrow (CO)_{ad} + 4H^+ + 4e^- \qquad (11)$$

$(CO)_{ad}$ represents an adsorbed CO species either on Pt or on Ru. Both Pt and Ru dissociate water to form adsorbed OH

$$Ru + H_2O \longrightarrow (OH)_{ad} + H^+ + e^- \qquad (12)$$

$$Pt + H_2O \longrightarrow (OH)_{ad} + H^+ + e^- \qquad (13)$$

Finally, following a Langmuir–Hinshelwood mechanism adsorbed CO reacts with adsorbed OH to give CO_2,

$$(CO)_{ad} + (OH)_{ad} \longrightarrow CO_2 + H^+ + e^- \qquad (14)$$

For CO adlayers obtained via adsorption of dissolved CO on PtRu, Koper *et al.*[95] analyzed reaction (14) for all possible species mentioned above and found that an enhanced effect is *only* possible if the final oxidation step occurs between CO adsorbed at Pt and OH adsorbed at Ru. Therefore, reaction (14) can be specifically written as

$$Pt(CO)_{ad} + Ru(OH)_{ad} \longrightarrow CO_2 + H^+ + e^- \qquad (15)$$

As a necessary condition for the Langmuir–Hinshelwood mechanism, CO should be able to diffuse on the surface. Koper *et al.*[95] found that the experimental results can be explained if the CO mobility on the surface is relatively high.

Besides the promoter effect of Ru through reaction (15), there is experimental evidence of additional effects of Ru on the reaction. The potentiodynamic curves (first sweep) of Figure 18, obtained at PtRu electrodeposits in the course of DEMS experiments, show a negative shift in the dissociative adsorption of methanol, depending on the Ru content of the electrodes. Further evidence of the earlier adsorption was obtained via infrared spectroscopy and are presented later. Also, the lowering of the CO adsorption energy for the alloy can contribute to the catalysts.[51]

For technical applications it is desirable that activating effects be sustained over long periods of time. Therefore, the results from basic experiments designed to judge

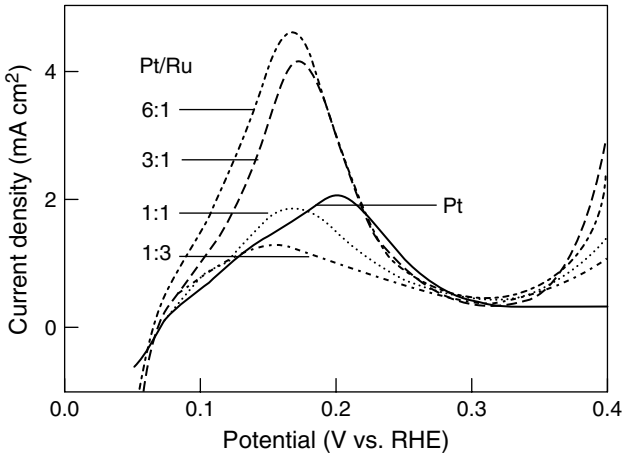

Figure 18. First potential scan in 1.0 M CH_3OH + 0.5 M H_2SO_4, starting at 50 mV (RHE); scan rate 1 mV s^{-1}. Porous electrodes prepared by depositing Pt and Ru at 0.2 V vs. RHE up to a total charge of 1200 mC, from solutions containing xmM $RuCl_3$ and ymM H_2Cl_6 Pt in 0.5 M H_2SO_4. The x/y ratios are indicated in each curve.

and compare the capability of PtRu materials are usually obtained in the form of current-time curves at constant potential. An example of *i-t* data obtained on different materials is given in Figure 19.[89, 90] Compared to pure Pt(111), the currents for the alloys are several orders of magnitude higher. Comparable results are reported by other authors under similar conditions.[84, 86, 87] Alloys used to obtain the data in Figure 19 were sputter cleaned and careful heated in UHV, following the pre-treatment technique suggested by Gasteiger *et al.*[96] This method for pre-treating the alloys produces surfaces presenting the same composition as the bulk. Besides this, the surface state is reproducible and the roughness factor is close to 1. This statement is supported by the fact that cyclic voltammograms for UHV cleaned alloys present current densities of the same order of magnitude as a Pt(111)/Ru electrode with the same Ru coverage, as expected for comparable smooth surfaces.[85]

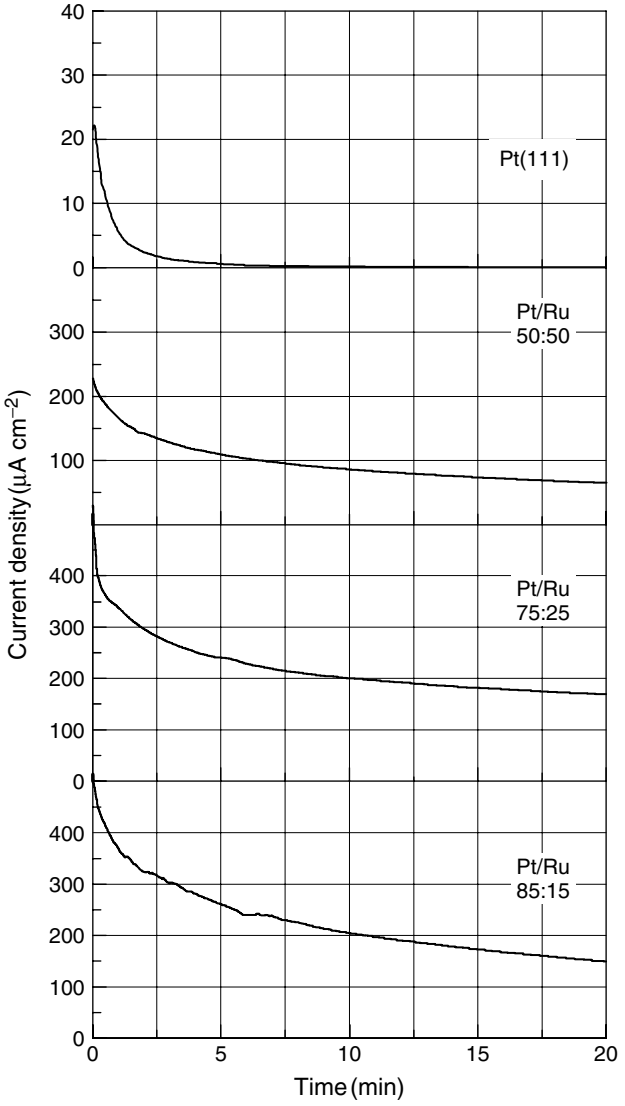

Figure 19. Current–time curves for comparing the catalytic activity of Pt(111) and PtRu alloys, towards methanol oxidation in 0.5 M CH_3OH + 0.1 M $HClO_4$. Potential 0.5 V vs. RHE. Room temperature, electrodes surfaces cleaned in UHV. (Reproduced from Hoster *et al.* (2001)[90] by permission from the Electrochemical Society.)

One intriguing effect is observed on all smooth PtRu materials: at constant potential in methanol solutions, they exhibit a decay of current as seen in Figure 19. The corresponding effect by constant current, namely an increase of overpotential with time, was reported by Hamnett *et al.*[74] In chronoamperometric experiments the current does not reach a stationary behavior even after several hours. Two different origins of this effect causing electrode deactivation have been identified. One of these is reversible and seems to be caused by the oxidation of the Ru surface,[74, 89, 90] since Ru oxides like RuO_2 and RuO_3 are not active as oxygen donors for CO oxidation. The electrode activity is thus partially recovered by applying a potential step towards more negative values, where the ruthenium oxides are reduced. The other factor causing the decay of current is, apparently, a blockage of the surface by some organic residue, which is slowly formed and can only be oxidized at high anodic potentials. However, no spectroscopic proofs are yet available on the nature of such blocking species.

The results of *i-t* curves obtained at room temperature for the two types of materials (alloys and Pt(111)/Ru) are collected in Figure 20, where the current at 0.5 V vs. RHE is plotted as a function of the Ru/Pt surface composition. It is noteworthy that in spite of the fact that the data for the alloys in this figure were measured in two different groups,[84, 85] they fit together nicely. Also, methanol oxidation on the PtRu alloys seems to be identical for H_2SO_4 and $HClO_4$, the two electrolytes used. Two main points can be extracted from this plot: (i) PtRu alloys are better catalysts than Pt(111)/Ru, and (ii) both materials present a wide maximum (between ca. 10–40% Ru for the alloy and ca. 15–50% for the Pt(111)/Ru electrodes) at room temperature.

In terms of the bi-functional mechanism, these maxima indicate that a Ru percentage of ca. 10–45% on the surface is enough to provide an efficient oxidation of adsorbed methanol residues. For compositions within the maxima, the quantity of Ru is not a limiting factor for the reaction. Therefore, within this range it should be possible to study the influence of other parameters (like, e.g., methanol concentration) on the reaction. Moreover, this region of Ru concentrations would be appropriate for studying the kinetics of the reaction. The upper limit of Ru coverage, on the other hand, is given by the necessity of having enough Pt sites for adsorbing and dissociating methanol. This limit

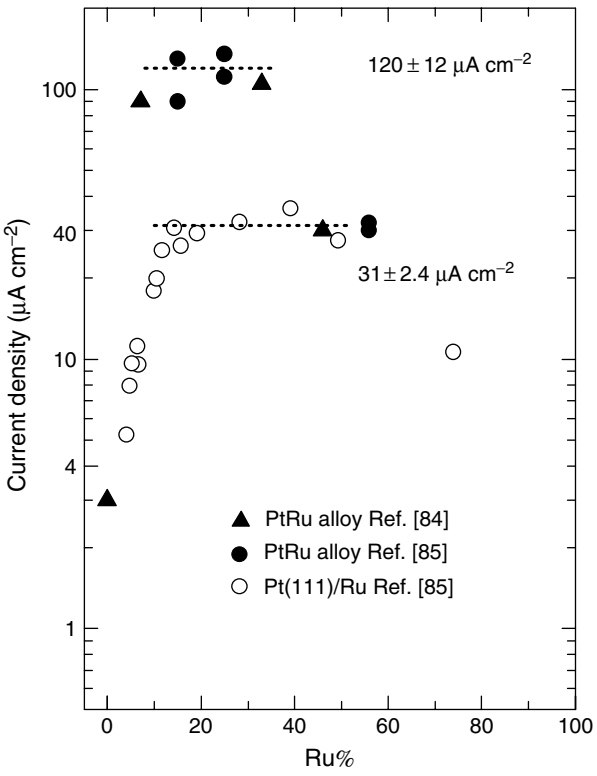

Figure 20. Plot of the current density for oxidation from current-time curves at 0.5 V as in Figure 19, as function of Ru coverage. Data for UHV prepared PtRu alloys, obtained at 20 min; data for Pt(111)/Ru formed by spontaneous adsorption were measured after 5 min. Solutions: 0.5 M H_2SO_4 + 0.5 M CH_3OH (data from Ref. [84]), 0.5 M CH_3OH + 0.1 M $HClO_4$ (data from Ref. [85]). (Reproduced from Iwasita *et al.*[85] © (2000) the American Chemical Society.)

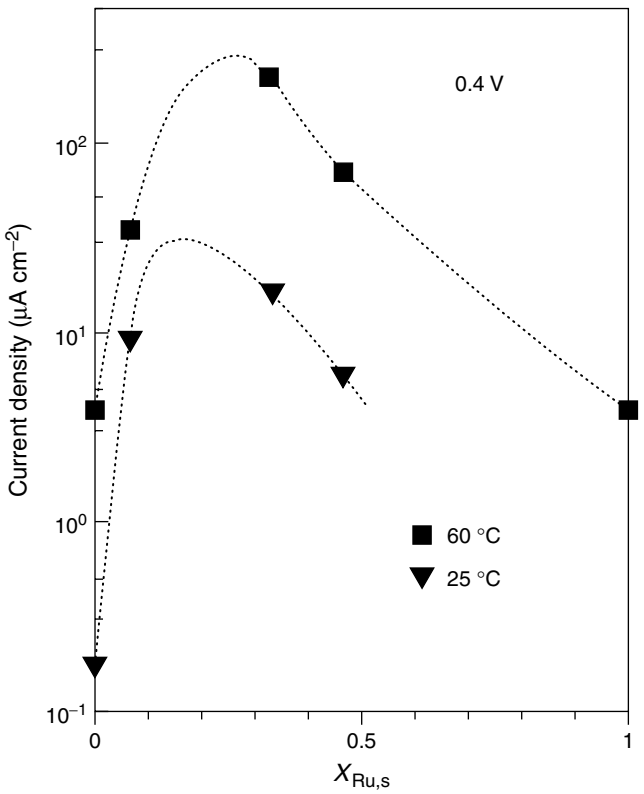

Figure 21. Current densities for methanol oxidation at 0.4 V in 0.5 M CH_3OH + 0.5 M H_2SO_4 vs. Ru surface composition of sputter cleaned Pt-Ru alloys. Electrode immersion at 0.075 V for 3 min prior to stepping to the indicated potential. Dashed lines are arbitrarily drawn smooth curves to connect the experimental data points. (Reproduced from Gasteiger *et al.* (1994)[84] by permission from The Electrochemical Society, Inc.)

is somewhat higher for adsorbed Ru than for the alloy (observe the wider maximum). This and the higher currents observed on the alloys may be related to the fact that the latter present a more homogeneous distribution of Ru atoms than the Pt(111)/Ru electrode. STM data of Pt(111)/Ru show that Ru tends to form aggregates (islands) on the surface of Pt.[89, 90] Thus, for the same Ru percentage, wider Pt patches can be found on the Pt(111)/Ru surface than on the alloy. It is noteworthy that with increasing temperature, the maximum of the $j-\theta_{Ru}$ plot for the alloy is shifted to somewhat higher θ_{Ru} values (Figure 21).[84] This effect probably originates in the fact that at higher temperatures (e.g., 60 °C), Ru becomes active for adsorbing and oxidizing methanol (see the value of current for pure Ru in Figure 21).

3.7.1 Spectroscopic results of methanol oxidation on PtRu materials

Further discussion on the Ru promoter effect requires a consideration of infrared spectroscopy and mass spectrometry data for PtRu electrodes.[82, 85] The spectra of Figure 22 for the PtRu alloy were obtained on UHV cleaned surfaces, as for the current time curves of Figure 19. The bands observed on both Pt(111)Ru and PtRu (85 : 15) alloy correspond to CO_2 (2341 cm^{-1}) and CO_L (2050 cm^{-1}). At Pt(111) a band at ca. 1820 cm^{-1} is due to bridge adsorbed (CO_B). Congruently with the higher currents observed on the alloys, the PtRu alloy electrode presents the highest production of CO_2 at a given potential (note the differences in scale). In the spectra of Figure 22 it is also noteworthy that at PtRu the band intensities for adsorbed CO remain approximately constant although the CO_2 production markedly increases with potential. This fact indicates that the CO intermediate reaches a stationary coverage, balancing the rates of formation and oxidation.

Although no features for other intermediates or soluble products were observed under the conditions for taking the spectra on the PtRu materials shown in Figure 22. DEMS experiments performed on a PtRu electrode in 1.0 M CH_3OH[82] do show the formation of $HCOOCH_3$

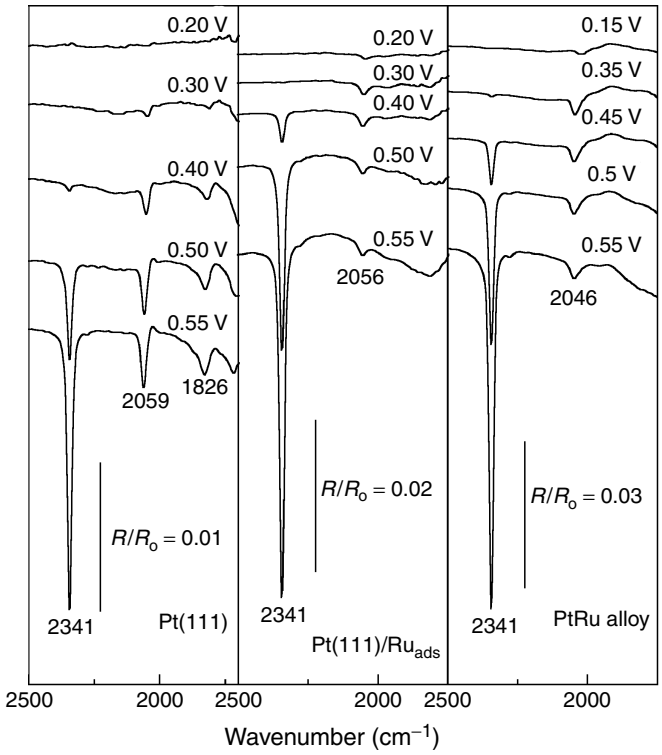

Figure 22. Comparison of in situ FTIR spectra for Pt(111), Pt(111)/Ru 39% and PtRu alloy (85 : 15) in 0.5 M CH_3OH + 0.1 M $HClO_4$. Potentials as indicated on each spectrum; reference spectrum taken at 0.05 V (from Ref. [85] with added spectra at 0.55 V). (Reproduced from Iwasita *et al.*[85] © (2000) the American Chemical Society.)

(Figure 23) as a soluble product. Other authors reported the presence of formaldehyde and formic acid in spectra obtained on PtRu alloys.[91] As previously indicated, the yields of different products on a Pt electrode depend on several experimental parameters such as methanol concentration and electrode roughness.[62] So far, IR spectra on well-prepared PtRu alloys in concentrated methanol solutions (above 0.5 M) have not been published and the question on the parallel paths on PtRu should be left open to further discussion.

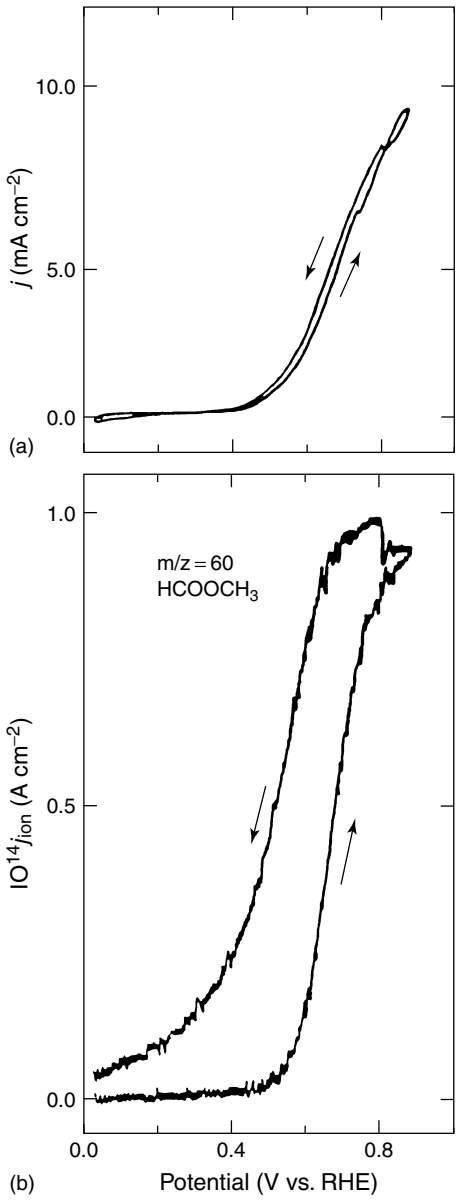

Figure 23. DEMS experiment on PtRu porous electrode in 1.0 M CH_3OH/0.5 M H_2SO_4; sweep rate: 20 mV s^{-1}. Electrode, electrodeposited Pt and Ru during 7 min at 0.05 V, on a gold substrate. Solution for electrodeposit, 10 mM $RuCl_3$ + 10 mM H_2Cl_6Pt in 0.5 M H_2SO_4.[82]

4 CONCLUDING REMARKS

In recent years, considerable progress has been made in the understanding of CO and methanol electrooxidation reactions and on their catalysis. In spite of its molecular simplicity, electrooxidation of carbon monoxide is a complex process, depending not only on the surface structure of the substrate but also on the potential at which the adsorption occurs. Stripping of a CO monolayer at Pt in pure supporting electrolyte requires high potentials (0.7–0.8 V). However, in the presence of dissolved CO and for low admission potentials (near 0.05 V), the first potential scan of a CV exhibits high currents starting at ca. 0.25 V. The current is shifted to higher anodic potentials in the subsequent scans, indicating that some irreversible surface transition occurs in the CO adlayer during the first incursion to higher positive potentials.

Bulk CO oxidation on Pt is catalyzed by nonmetal adatoms such as S, Se, Te, up to high degrees of coverage by the adatom. The catalytic effect increases with increasing

adatom electronegativity. However, none of these adatoms catalyses methanol oxidation.

As for other small organic molecules, parallel pathways occur during methanol oxidation. In addition to CO_2 which is the major product at low potentials and low concentrations, formic acid (methyl formate) and formaldehyde are other soluble reaction products, their yields depending on experimental conditions such as surface roughness and methanol concentration.

In spite of noticeable structural effects on the Pt surface, which are reflected on the amount and rate of surface blocking by CO, comparable "quasi-stationary" rates of CO_2 production are observed at Pt(111) and Pt(110) in the potential region between ca. 0.4 V and 0.8 V. This result, which is valid for CH_3OH concentrations >0.3 M, indicates that the rate-determining process for the $6e^-$ reaction is the oxidation of the adsorbed species and not the adsorption of methanol.

At room temperature PtRu alloys with a Ru content between 10% and 40% are, at present, the best catalysts for the reaction. This is probably due to a good distribution of Pt and Ru atoms as compared to other materials where the atoms tend to segregate forming patches of pure Ru or Pt, thus physically separating the bi-functional partners. Experimental data show that the mechanism of catalysis is not due only to a bi-functional action of both metals. Other effects, such as lowering the potential for methanol adsorption also seem to be of importance.

Some deactivation effects are observed during polarization at constant potential on smooth electrodes, the origin of these probably being the formation of inactive ruthenium oxides and blockage of the surface by organic residues of unknown nature.

REFERENCES

1. W. Vielstich, 'Fuel Cells', Wiley Interscience, New York (1965).
2. M. W. Breiter, 'Electrochemical Processes in Fuel Cells', Springer-Verlag, Berlin (1969).
3. O. A. Petrii, B. I. Podlovchenko, A. N. Frumkin and H. Lal, *J. Electroanal. Chem.*, **10**, 253 (1965).
4. V. S. Bagotzki and Yu. Vassileiv, *Electrochim. Acta*, **12**, 1323 (1967).
5. M. Breiter, *Electrochim. Acta*, **12**, 1213 (1967).
6. V. S. Bagotzki, Yu. B. Vassiliev and O. A. Kazova, *J. Electroanal. Chem.*, **81**, 229 (1977).
7. O. A. Petrii, B. I. Podlovchenko, A. N. Frumkin and H. Lal, *J. Electroanal. Chem.*, **10**, 253 (1965).
8. K. J. Cathro, *J. Electrochem. Soc.*, **116**, 1608 (1969).
9. M. M. P. Janssen and J. Moolhuysen, *J. Catal.*, **46**, 289 (1977).
10. G. Sandstede, 'From Electrocatalysis to Fuel Cells', University of Washington, Seattle, WA (1972).
11. T. Iwasita, in 'Advances in Electrochemical Science and Engineering', H. Gerischer and Ch. Tobias (Eds), Verlag Chemie, Vol. 1, p. 127 (1990).
12. B. Beden, C. Lamy, A. Bewick and K. Kunimatsu, *J. Electroanal. Chem.*, **121**, 343 (1981).
13. (a) O. Wolter, C. Giordano, J. Heitbaum and W. Vielstich, 'Proc. Symp. Electrocatalysis', The Electrochemical Society, Pennington, NJ, p. 235 (1982); (b) B. Bittins-Cattaneo, E. Cataneo, P. Königshoven and W. Vielstich, in 'Electroanalytical Chemistry: A Series of Advances', A. J. Bard (Ed), Marcel Dekker, New York, p. 18 114 (1991).
14. T. Iwasita and F. C. Nart, in 'Progress in Surface Science', S. G. Davison (Ed), Pergamon, Oxford, Vol. 55, p. 271 (1997).
15. J. Clavilier, D. Armand, S. G. Sun and M. Petit, *J. Electroanal. Chem.*, **205**, 267 (1986).
16. R. Parsons and T. Van der Not, *J. Electroanal. Chem.*, **257**, 1 (1988).
17. S. Wasmus and A. Küver, *J. Electroanal. Chem.*, **461**, 14 (1999).
18. A. Hamnett, in 'Interfacial Electrochemistry. Theory, Experimental and Applications', A. Wieckowski (Ed), Marcel Dekker, New York, p. 843 (1999).
19. I. Villegas and M. J. Weaver, *J. Chem. Phys.*, **101**, 1648 (1994).
20. K. Yoshimi, M.-B. Song and M. Ito, *Surf. Sci.*, **368**, 389 (1996).
21. I. Villegas and M. J. Weaver, *J. Phys. Chem. B*, **101**, 10 166 (1997).
22. N. Kizhakevarian, I. Villegas and M. J. Weaver, *J. Phys. Chem.*, **99**, 7677 (1995).
23. F. T. Wagner, in 'Structure of Electrified Interfaces', J. Lipkowski and P. N. Ross (Eds), VCH, New York, Chapter 9 (1993).
24. H. A. Gasteiger, N. Markovic and P. N. Ross, *J. Phys. Chem.*, **99**, 8290 (1995).
25. R. I. Masel, 'Principles of Adsorption and Reaction at Surfaces', Wiley-Interscience, New York (1996).
26. R. Ducros and R. P. Merill, *Surf. Sci.*, **55**, 227 (1976).
27. C. Gutiérrez and A. J. Caram, *J. Electroanal. Chem.*, **305**, 259 (1991); A. J. Caram and C. Gutiérrez, *J. Electroanal. Chem.*, **308**, 321 (1991).
28. E. P. M. Leiva, C. Giordano, R. M. Cervino and A. J. Arvia, *J. Electrochem. Soc.*, **133**, 1660 (1986).
29. F. Kitamura, M. Taijedo, M. Takahashi and M. Ito, *Chem. Phys. Lett.*, **142**, 349 (1986).
30. A. Couto, M. C. Pérez, A. Rincón and C. Gutiérrez, *J. Phys. Chem.*, **100**, 19 538 (1996).
31. A. Wieckowski, M. Rubel and C. Gutiérrez, *J. Electroanal. Chem.*, **382**, 97 (1995).

32. K. Kunimatsu, H. Seki, W. G. Gordon, J. G. Gordon II and M. R. Philpot, *Langmuir*, **2**, 464 (1986).
33. H. Kita, K. Shimatsu and K. Kunimatsu, *J. Electroanal. Chem.*, **241**, 163 (1988).
34. N. M. Marković, C. A. Lucas, B. N. Grgur and P. N. Ross, *J. Phys. Chem. B*, **103**, 487 (1999).
35. H. Kita, H. Narumi, S. Ye and H. Naohara, *J. Appl. Electrochem.*, **23**, 589 (1993).
36. G. Ertl, M. Newmann and K. M. Streit, *Surf. Sci.*, **64**, 101 (1977).
37. S. Gilman, *J. Phys. Chem.*, **68**, 70 (1964).
38. C. T. Campbell, G. Ertl, H. Kuipers and J. Segner, *J. Chem. Phys.*, **73**, 5862 (1980).
39. M. T. M. Koper, A. P. J. Jansen, R. A. van Santen, J. J. Lukkien and P. A. J. Hibers, *J. Chem. Phys.*, **109**, 6051 (1998).
40. B. Love and J. Lipkowski, in 'Electrochemical Surface Science, Molecular Phenomena at Electrode Surfaces', P. M. Soriaga (Ed), ACS Symposium Series, ACS, Washington, DC, p. 484 (1988).
41. C. McCallum and D. Pletcher, *J. Electroanal. Chem.*, **70**, 277 (1976).
42. E. Santos, E. P. M. Leiva and W. Vielstich, *Electrochim. Acta*, **36**, 555 (1990).
43. A. V. Petukhov, W. Ackerman, K. A. Friedrichs and U. Stimming, *Surf. Sci.*, **402–404**, 182 (1998).
44. A. Rodes, R. Gómez, J. M. Feliu and M. J. Weaver, *Langmuir*, **16**, 811 (2000).
45. W. Ackerman, K. A. Friedrich, U. Linke and U. Stimming, *Surf. Sci.*, **402**, 571 (1998).
46. H. Binder, H. Köhnling and G. Sandstede, *Adv. Energy Conversion*, **7**, 77 (1967).
47. M. Shibata and S. Motoo, *J. Electroanal. Chem.*, **194**, 261 (1985); **194**, 275 (1985).
48. M. Watanabe, Y. Furuuchi and S. Motoo, *J. Electroanal. Chem.*, **192**, 367 (1985).
49. V. D. Thomas, J. W. Schwank and J. L. Gland, *Surf. Sci.*, **464**, 153 (2000).
50. T. E. Fischer and S. R. Kelemen, *Surf. Sci.*, **69**, 1 (1977).
51. F. Christoffersen, P. Liu, A. Ruban, H. L. Skriver and J. K. Nørskov, *J. Catal.*, **199**, 123 (2001); B. Hammer and J. K. Nørskov, *Surf. Sci.*, **343**, 211 (1995).
52. H. Herrero, A. Rodes, J. M. Pérez, J. M. Feliu and A. Aldaz, *J. Electroanal. Chem.*, **412**, 165 (1996).
53. M. P. Kiskinova, A. Szabò and T. J. Yates, Jr, *Surf. Sci.*, **226**, 237 (1990).
54. T. Iwasita and X. Xia, *J. Electroanal. Chem.*, **411**, 95 (1996).
55. T. Iwasita, X. H. Xia, H. D. Ließ and W. Vielstich, *J. Phys. Chem. B*, **101**, 7542 (1997).
56. T. Iwasita and F. C. Nart, *J. Electroanal. Chem.*, **317**, 291 (1991).
57. S. Wilhelm, T. Iwasita and W. Vielstich, *J. Electroanal. Chem.*, **238**, 383 (1987).
58. X. H. Xia, T. Iwasita, F. Ge and W. Vielstich, *Electrochim. Acta*, **41**, 711 (1996).
59. T. O. Pavela, *Ann. Acad. Sci. Fenn. Ser. K.*, **A2**, 1 (1954).
60. M. J. Schlatter, in 'Fuel Cells', G. Y. Yong (Ed), Reinhold, New York, p. 199 (1963).
61. M. Breiter, *Discuss. Faraday Soc.*, **45**, 79 (1968).
62. K.-I. Ota, Y. Nakagawa and M. Takahashi, *J. Electroanal. Chem.*, **179**, 179 (1984).
63. (a) H. Wang, T. Löffler and H. Baltruschat, *J. Appl. Electrochem.*, **31**, 759 (2001); (b) H. Wang, C. Wingender, H. Baltruschat and M. Lopez, *J. Electroanal. Chem.*, **509**, 163 (2001).
64. S. Wasmus, J.-T. Wang and R. F. Savinell, *J. Electrochem. Soc.*, **142**, 3825 (1995).
65. C. Korzeniewski and C. Childers, *J. Phys. Chem. B*, **102**, 489 (1998).
66. T. Iwasita and W. Vielstich, *J. Electroanal. Chem.*, **401**, 203 (1986).
67. N. Markovic and P. N. Ross, *J. Electroanal. Chem.*, **330**, 499 (1992).
68. H. Kita, Y. Gao and H. Hattori, *J. Electroanal. Chem.*, **373**, 177 (1994).
69. P. Faguy, N. Markovic, R. Adzic, C. Fierro and E. Yeager, *J. Electroanal. Chem.*, **289**, 1247 (1990).
70. F. C. Nart, T. Iwasita and M. Weber, *Electrochim. Acta*, **39**, 961 (1994); T. Iwasita, F. C. Nart and M. Weber, *Electrochim. Acta*, **39**, 2093 (1994).
71. H. A. Gasteiger, N. Markovic, P. N. Ross and E. J. Cairns, *J. Phys. Chem.*, **97**, 12 020 (1993).
72. P. A. Christensen, A. Hamnett and G. L. Troughton, *J. Electroanal. Chem.*, **362**, 207 (1993).
73. H. Kim, I. Rabelo de Moraes, G. Tremiliosi-Filho, R. Haasch and A. Wieckowski, *Surf. Sci.*, **474**, L203 (2001).
74. A. Hamnett, S. A. Weeks, B. J. Kennedy, G. Troughton and P. A. Christensen, *Ber. Bunsen-ges. Phys. Chem.*, **94**, 1014 (1990).
75. S. A. Campbell and R. Parsons, *J. Chem. Soc. Farad. Trans.*, **88**, 833 (1992).
76. H. Kita, H. Nakajima and K. Shimazu, *J. Electroanal. Chem.*, **248**, 181 (1988).
77. H. Binder, A. Köhling and G. Sandstede, in 'From Electrocatalysis to Fuel Cells', G. Sandstede (Ed), University of Washington, Seattle, WA (1972).
78. M. Watanabe and S. Motoo, *J. Electroanal. Chem.*, **69**, 429 (1976).
79. T. Iwasita, F. C. Nart and W. Vielstich, *Ber. Bunsen-ges. Phys. Chem.*, **94**, 1030 (1990).
80. M. Watanabe and S. Motoo, *J. Electroanal. Chem.*, **60**, 267 (1975).
81. T. Frelink, W. Visscher, A. P. Cox and J. A. R. van Veen, *Electrochim. Acta*, **40**, 1537 (1995).
82. M. Krausa and W. Vielstich, *J. Electroanal. Chem.*, **379**, 307 (1994).
83. N. Markovic, H. A. Gasteiger, P. N. Ross, L. Villegas and M. J. Weaver, *Electrochim. Acta*, **40**, 91 (1995).

84. H. A. Gasteiger, N. Markovic, P. N. Ross and E. J. Cairns, *J. Electrochem. Soc.*, **141**, 1795 (1994).

85. T. Iwasita, H. Hoster, A. John-Anacker, W. F. Lin and W. Vielstich, *Langmuir*, **16**, 522 (2000).

86. W. Chrzanowski and A. Wieckowski, *Langmuir*, **14**, 1967 (1998).

87. W. Chrzanowski, W. H. Kim and A. Wieckowski, *Catal. Lett.*, **50**, 69 (1998).

88. G. Tremiliosi-Filho, H. Kim, W. Chrzanowski, A. Wieckowski, B. Grzybowska and P. Kulesza, *J. Electroanal. Chem.*, **467**, 143 (1999).

89. H. Hoster, T. Iwasita, H. Baumgärtner and W. Vielstich, *Phys. Chem. Chem. Phys.*, **3**, 337 (2001).

90. H. Hoster, T. Iwasita, H. Baumgärtner and W. Vielstich, *J. Electrochem. Soc.*, **148**, A496 (2001).

91. A. Kabbaby, R. Faure, R. Durand, B. Beden, F. Hahn, J.-M. Leger and C. Lamy, *J. Electroanal. Chem.*, **444**, 41 (1998).

92. W. H. Lizcano-Valbuena, E. C. Bortholin, A. Oliveira Neto, V. A. Paganin and E. R. González, '200th Meeting of the Electrochemical Society, 52nd ISE Meeting', Electrochemical Society, Pennington, NJ, Ext. Abstract 330 (2001).

93. A. O. Neto, J. Peres, W. T. Naporn, E. Ticcianelli and E. González, *J. Braz. Chem. Soc.*, **11**, 39 (2000).

94. D. Kardash, C. Korzeniewski and N. Markovic, *J. Electroanal. Chem.*, **500**, 518 (2001).

95. M. T. M. Koper, J. J. Lukkien, A. P. J. Jansen and R. A. van Santen, *J. Phys. Chem. B*, **103**, 5522 (1999).

96. H. A. Gasteiger, P. N. Ross and E. J. Cairns, *Surf. Sci.*, **293**, 67 (1993).